PNAS

Supporting Information for

A peptidomimetic modulator of the $Ca_V2.2$ N-type calcium channel for chronic pain

Kimberly Gomez[1,2†], Ulises Santiago[3†], Tyler S. Nelson[1,2], Heather N. Allen[1,2], Aida Calderon-Rivera[1,2], Sara Hestehave[1,2], Erick J. Rodríguez Palma[1,2], Yuan Zhou[4], Paz Duran[1,2], Santiago Loya-Lopez[1,2], Elaine Zhu[5,6], Upasana Kumar[7], Rory Shields[8], Eda Koseli[9], Bryan McKiver[9], Denise Giuvelis[10], Wanhong Zuo[11], Kufreobong E. Inyang[12], Angie Dorame[4], Aude Chefdeville[4], Dongzhi Ran[13], Samantha Perez-Miller[1,2], Yi Lu[13], Xia Liu[13], Handoko[14], Paramjit S. Arora[14], Marcel Patek[15], Aubin Moutal[16], May Khanna[1,2], Huijuan Hu[11], Geoffroy Laumet[12], Tamara King[10], Jing Wang[5,6,17], M. Imad Damaj[9], Olga A. Korczeniewska[7,8], Carlos J. Camacho[3,*], and Rajesh Khanna[1,2,17,18,*]

[1]Department of Molecular Pathobiology, College of Dentistry, New York University, 433 First Avenue, 8th floor, New York, NY, 10010, USA
[2]NYU Pain Research Center, 433 First Avenue, New York, NY 10010, USA
[3]Department of Computational and Systems Biology, University of Pittsburgh, Pittsburgh, PA, 15261, USA
[4]Department of Pharmacology, College of Medicine, University of Arizona, Tucson, AZ 85724, USA
[5]Department of Anesthesiology, Perioperative Care and Pain Medicine, New York University Grossman School of Medicine, New York, NY, 10016, USA
[6]Interdisciplinary Pain Research Program, New York University Langone Health, New York, NY 10016 USA
[7]Center for Orofacial Pain and Temporomandibular Disorders, Department of Diagnostic Sciences, Rutgers School of Dental Medicine, Newark, NJ 07101, USA
[8]Rutgers School of Graduate Studies, Newark Health Science Campus, Newark, NJ 07101, USA
[9]Department of Pharmacology and Toxicology and Translational Research Initiative for Pain and Neuropathy, Virginia Commonwealth University, USA.
[10]Department of Biomedical Sciences, College of Osteopathic Medicine, Center for Excellence in the Neurosciences, University of New England, Biddeford, Maine 04005
[11]Department of Anesthesiology, Rutgers New Jersey Medical School, 185 S. Orange Ave., MSB, E-661, Newark, NJ 07103, USA
[12]Department of Physiology, Michigan State University, East Lansing, MI, 48824, USA
[13]Department of Pharmacology, School of Pharmacy, Chongqing Medical University, Chongqing 400016, China
[14]Department of Chemistry, New York University, 100 Washington Square East, New York, NY 10003, USA
[15]Bright Rock Path LLC, Tucson, Arizona, USA
[16]Department of Pharmacology and Physiology, School of Medicine, St. Louis University, St. Louis, MO, 63104, USA.
[17]Department of Neuroscience and Physiology and Neuroscience Institute, School of Medicine, New York University, New York, NY, 10010, USA.
[18]Chemical, and Biomolecular Engineering Department, Tandon School of Engineering, New York University, 6 Metrotech Center, Brooklyn, NY 11201

[†]Contributed equally to this work

*Correspondence to:
Dr. Rajesh Khanna, Department of Molecular Pathobiology, College of Dentistry, New York University, 433 First Avenue, 8th floor, New York, NY, 10010, USA. Office phone: (520) 271-0433; Email: rk4272@nyu.edu or

Dr. Carlos J. Camacho, Department of Computational and Systems Biology, University of Pittsburgh, Pittsburgh, PA, 15261, USA. Email: ccamacho@pitt.edu

This PDF file includes:

SI Materials and Methods:
Figures S1 to S14
Tables S1 to S2
SI References

Supporting Information

SI Materials and Methods

Study Design. Detailed descriptions of experiments and associated references are available in SI Materials and Methods. This study was designed with the aim of developing selective blockers of $Ca_v2.2$ channels for use against chronic pain. Capitalizing on the demonstrated regulation of $Ca_v2.2$ by the auxiliary protein CRMP2, we focused our efforts on designing a small molecule to emulate the antinociceptive CRMP2-derived peptide we previously reported to uncouple the $Ca_v2.2$-CRMP2 interaction. To identify a peptidomimetic of this peptide, we developed and applied a novel molecular dynamics approach to identify the $Ca_v2.2$ recognition motif of the core peptide, used its presenting motif to design pharmacophore models to screen 27 million compounds in the open access server ZincPharmer. We used biochemical approaches to validate the interaction in cultured cells and investigated the effects of disrupting this interaction on $Ca_v2.2$ trafficking. We used electrophysiological approaches to test the functional consequences of disrupting this interaction in DRG neurons and spinal cord slices. Furthermore, we investigated the effects of our disruption strategy in naïve animals as well as in three neuropathic pain and an inflammatory model to assay the off-target and on-target actions of this approach. Four routes of administration were used, including intraperitoneal, intrathecal, intraplantar, and intranasal. All electrophysiology, biochemistry, in vivo fiber photomometry, and behavior experiments were performed according to established protocols (1). All animal protocols were approved by the Institutional Animal Care and Use Committee of the College of Medicine at the University of Arizona, College of Osteopathic Medicine, New York University Grossman School of Medicine, Virginia Commonwealth University, Rutgers New Jersey Medical School, Michigan State University, and Rutgers School of Dental Medicine, and conducted in accordance with the Guide for Care and Use of Laboratory Animals published by the National Institutes of Health. Sample sizes were determined based on our experience with electrophysiological, biochemical, and behavioral experiments in our laboratory. Experimenters were blind to the treatment and the animals were randomly assigned to experimental groups.

Rational design of pharmacophore models in the absence of receptor structure.

Molecular dynamics of CBD3 peptide. We modeled the CBD3 peptide based on the X-ray diffraction structure of CRMP2 (PDB: 5MKV) (2). Three independent molecular dynamics simulations (MDS) of both the CBD3 by itself and conjugated with a blood-brain barrier-permeable peptide TAT-CBD3 were run with pmemd.cuda (3-5) from AMBER18 using AMBER ff14SB force field (6). We used tLeap binary (AMBER18) for solvating the peptides in an octahedral TIP3P water box with a 15 Å distance from structure surface to the box edges, and closeness parameter of 0.75 Å. The neutralized system was solvated in a solution of 150 mM NaCl. H-bonds were constrained using SHAKE algorithm and integration time-step at 2 fs. Simulations were carried out equilibrating the system for 1 ns at NPT using Berstein barostat to keep constant pressure at 1 atm at 300K, followed by 300 ns NPT production at 300 K. The first 60 ns of each MDS were discarded as equilibration time.

Anchor prediction. Hierarchical clustering (7) determined the most stable conformation of dipeptides between A_1 and L_5. Clustering is based on the Root Mean Square Deviation (RMSD) between MDS

snapshots less than 1 Å for A_1R_2, R_2S_3, S_3R_4, and R_4L_5. We also determined the contacts of side chains as a proxy for ability to bind the receptor, i.e., if side chains are interacting with each other, their interaction with the receptor is hindered. Atomic contacts are defined as atoms from the peptide that are less than 3.8 Å of Cβ-alanine, [Nε, NH2]-arginine, Cβ-serine, [Cδ1, Cδ2]-leucine from dipeptides. The prediction is that the stable motif accessible to solvent is critical for molecular recognition, i.e., the anchor of the protein-protein interaction (8).

Virtual screening of ZINC database. We used the anchor motif as template to design and refine pharmacophore models to virtually screen more than 27 million compounds using the public server ZINCPharmer (9). Based on A_1R_2 configuration we screened near to 27 million commercially available compounds using ZINCPharmer, resulting in the compounds studied here. Small molecule conformations are sampled using Omega2 (10).

Synthesis of CBD3063

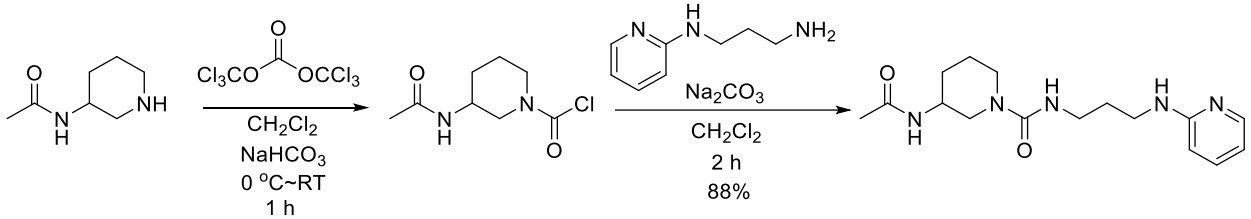

Step 1. 3-acetamidopiperidine-1-carbonyl chloride

In a cooled (0 °C) solution of *N*-(piperidin-3-yl)acetamide (500 mg, 3.52 mmol) in anhydrous dichloromethane (20 mL) was added $NaHCO_3$ (1.10 g, 10.6 mmol) and triphosgene (696 mg, 2.34 mmol). The mixture was stirred at room temperature for 1 hour. After all starting material has been consumed, the mixture was filtered, and the collected filtrate was evaporated under reduced pressure. The resulting residue was then allowed to passed through a short silica plug (wash with 100% EtOAc) to yield crude 3-acetamidopiperidine-1-carbonyl chloride (467 mg, 65%) as sticky transparent liquid (HRMS calcd for $C_8H_{14}ClN_2O_2^+$ $[M+H]^+$: 205.0748; found: 205.0738). The compound was used immediately for the next step without further purification.

Step 2. 3-acetamido-*N*-(3-(pyridin-2-ylamino)propyl)piperidine-1-carboxamide

3-acetamidopiperidine-1-carbonyl chloride (100 mg, 0.489 mmol) from the previous step was dissolved in anhydrous dichloromethane (5.0 mL). Into this solution was added Na_2CO_3 (104 mg, 0.977 mmol) and N^1-(pyridin-2-yl)propane-1,3-diamine (73.9 mg, 0.489 mmol). The mixture was stirred for 2 hours, upon which all starting material had reacted. The mixture was filtered, and the collected filtrate was evaporated under reduced pressure. The resulting residue was then purified by flash column chromatography (gradient elution of 0% to 10% MeOH in CH_2Cl_2) to yield **3-**acetamido-*N*-(3-(pyridin-2-ylamino)propyl)piperidine-1-carboxamide (137 mg, 88%) as white foam solid. ^{1}H NMR (600 MHz, $CDCl_3$) δ 7.99 (dd, *J* = 4.1, 0.8 Hz, 1H), 7.38 (ddd, *J* = 8.7, 7.1, 1.9 Hz, 1H), 6.53 (ddd, *J* = 7.0, 5.2, 0.8 Hz, 1H), 6.41 (d, *J* = 8.4 Hz, 1H), 6.12 (d, *J* = 6.5 Hz, 1H), 5.79 (t, *J* = 5.5 Hz, 1H), 5.10 – 4.95 (m, 1H), 3.99 – 3.86 (m, 1H), 3.45 – 3.36 (m, 6H), 3.32 (q, *J* = 6.1 Hz, 2H), 1.95 (s, 3H), 1.87 – 1.62 (m, 5H), 1.61 – 1.49 (m, 1H). ^{13}C NMR (151 MHz, $CDCl_3$) δ 170.10, 158.60, 158.46, 147.02, 137.59, 112.50, 108.28, 48.66, 45.61, 44.60, 38.63, 37.69, 30.22, 29.40, 23.37, 22.23. HRMS calcd for $C_{16}H_{25}N_5O_2Na$ $[M+Na]^+$: 342.1900; found: 342.1908 (see NMR spectra below).

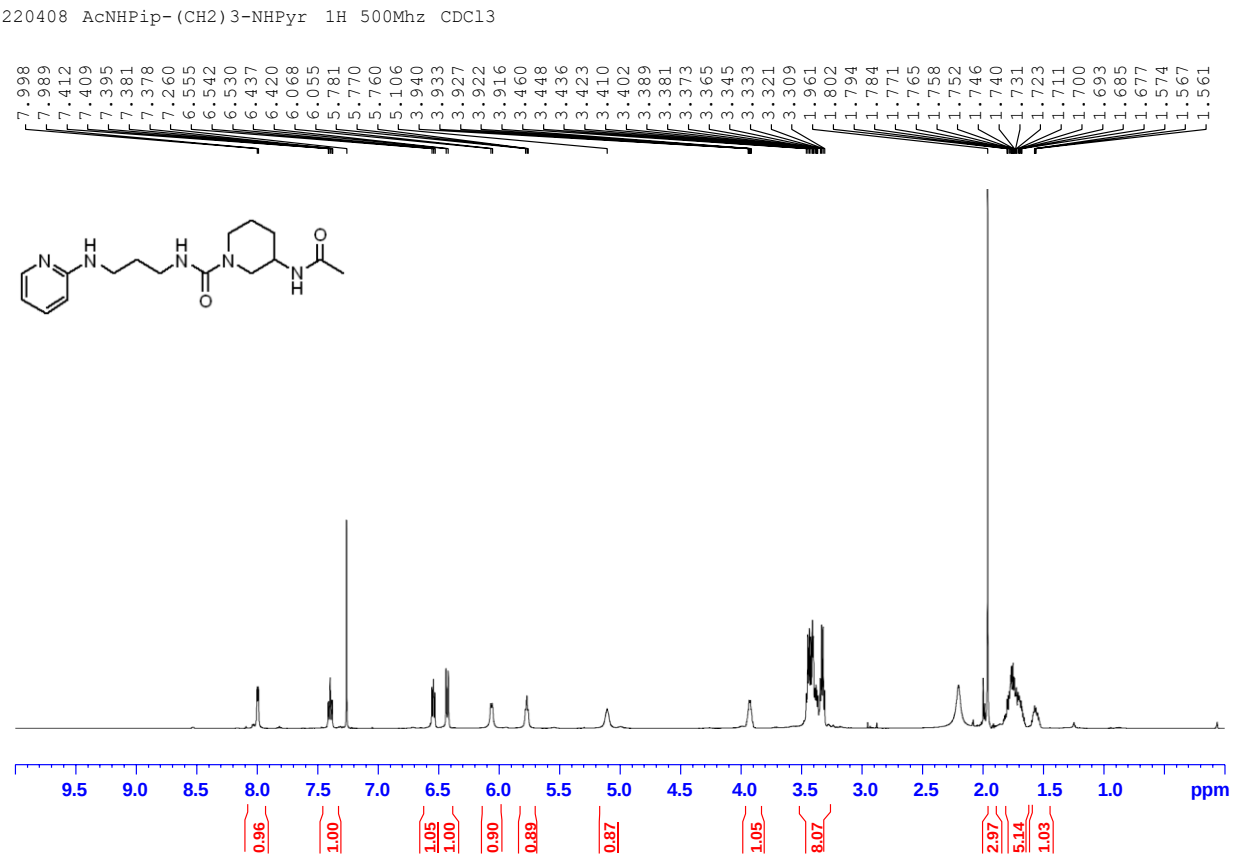

Culturing of CAD cell lines. Mouse neuron derived Cathecholamine A differentiated (CAD) cells (ECACC Cat# 08100805, RRID: CVCL_0199) were grown in standard cell culture conditions, 37 °C in 5% (vol/vol) CO_2. The cells were maintained in DMEM/F12 media supplemented with 10% (vol/vol) FBS (HyClone) and 1% penicillin/streptomycin sulfate from 10,000 µg/mL stock.

Immunoprecipitation (IP) of endogenous CRMP2 and SUMOylation. CAD cells were incubated overnight with vehicle (0.1 % DMSO) or CBD3063 (20 µM). The next day the cells were lysed into the IP buffer containing 20 mM Tris-HCl pH=7.4, 50 mM NaCl, 2 mM $MgCl_2$, 10 mM N-Ethylmaleimide (NEM), 1% (vol/vol) NP-40, 0.5% (mass/vol) sodium deoxycholate, 0.1% (mass/vol) sodium dodecyl sulfate (SDS) with protease inhibitors (Cat# B14002, Selleck, Houston, TX), phosphatase inhibitors (Cat# B15002, Selleck, Houston, TX) and Nuclease (Cat# 88701, Thermo Fisher Scientific, Waltham, MA). Total protein concentration was determined by BCA protein assay kit (Cat# PI23225, Thermo Fisher Scientific, Waltham, MA). Five hundred micrograms of total protein were incubated overnight with 2 µg of CRMP2 antibody (Cat# C2993, Sigma-Aldrich, St. Louis, MO) at 4°C under gentle agitation. For IP of SUMOylated CRMP2, CAD cells were transfected by using Lipofectamine 2000 (Cat# 11668019; Thermo Fisher Scientific, Waltham, MA) according to the manufacturer's instructions with 2.5 µg/µL pdsRed2-CRMP2 plasmid as previously described (11). 48 h after transfection, CAD cells were lysed into the IP buffer and 0.5% SDS was added to the lysates at 0.5% (mass/vol) final concentration, before boiling them for 5 min at 95 °C. Next, five hundred micrograms of total proteins were incubated with 5 µg of SUMO1 antibody (Cat# S8070; Sigma-Aldrich, St. Louis, MO) overnight at 4 °C under gentle agitation. Protein G magnetic beads (Cat# 10004D, Thermo Fisher Scientific, Waltham, MA), pre-equilibrated with the immunoprecipitation buffer, were then added to the lysates and incubated for 2 h at 4°C to capture immuno-complexes. Beads were washed four times with IP buffer to remove nonspecific binding of proteins, before resuspension in Laemmli buffer and boiling at 95°C for 5 min prior to immunoblotting.

Immunoblot preparation and analysis. Indicated samples were loaded on 4–20% Novex gels (Cat# XP04205BOX; Thermo Fisher Scientific, Waltham, MA). Proteins were transferred to preactivated

polyvinylidene difluoride (PVDF) membranes for 1 h at 100 V using TGS [25 mM Tris, pH 8.5, 192 mM glycine, 0.1% (mass/vol) SDS], 20% (vol/vol) methanol as transfer buffer (0.45 µm; Cat# IPVH00010; Millipore Sigma, St. Louis, MO). After transfer, the membranes were blocked at room temperature for 1 h with TBST (50 mM Tris·HCl, pH 7.4, 150 mM NaCl, 0.1% Tween 20) with 5% (mass/vol) nonfat dry milk, and then incubated overnight at 4 °C separately with indicated primary antibodies (1:1,000 dilution), βIII-Tubulin (Cat# G7121, Research Resource Identifiers (RRID):AB_430874; Promega, Madison, WI), CRMP2 (Cat# C2993, RRID:AB_1078573; Sigma-Aldrich, St. Louis, MO), Cav2.2 (Cat# TA308673, RRID:AB_2650547; Origene, Rockville, MD), CRMP2 pSer522 (Cat# CP2191, RRID:AB_2094486; ECM Biosciences, Versailles, KY), CRMP2 pT555 (Cat# CP2251, RRID:AB_2094483; ECM Biosciences, Versailles, KY), CRMP2 pThr514 (Cat# PA5-110113, RRID:AB_2855524; Thermo Fisher Scientific, Waltham, MA), in TBST, 5% (mass/vol) BSA. Following incubation in HRP-conjugated secondary antibodies from Jackson Immuno Research (West Grove, PA) (1:10,000 dilution), Mouse Anti-Rabbit (Cat# 211-032-171, RRID:AB_2339149) and Goat Anti-Mouse (Cat# 115-035-174, RRID:AB_2338512), blots were revealed by enhanced luminescence (WBKLS0500; Millipore Sigma St. Louis, MO). For examining the effect of CBD3063 on CRMP2 phosphorylation state, CAD cells were treated overnight with vehicle (0.1 % DMSO) or CBD3063 (20 µM) and the next day cells were lysed using RIPA buffer containing 20 mM Tris-HCl pH=7.4, 50 mM NaCl, 2 mM MgCl2, 1% (vol/vol) NP-40, 0.5% (mass/vol) sodium deoxycholate, 0.1% (mass/vol) sodium dodecyl sulfate (SDS) with protease inhibitors (Cat# B14002, Selleck, Houston, TX), phosphatase inhibitors (Cat# B15002, Selleck, Houston, TX) and Nuclease (Cat# 88701, Thermo Fisher Scientific, Waltham, MA). Approximately 40 µg of total proteins were loaded on an SDS-PAGE.

Animals.

Rats: Pathogen-free rats were kept in light (12-h light: 12-h dark cycle; lights on at 07:00 h) and temperature (23 ± 3°C) controlled rooms. Adult female Sprague-Dawley rats (~200 g, Charles River Laboratories, Wilmington, MA.) were used for immunocytochemistry, confocal microscopy and calcium imaging experiments. Female Sprague-Dawley rats (~75-100 g, Charles River Laboratories, Wilmington, MA.) were employed for DRG electrophysiological recordings. Male Sprague-Dawley rats (250 g, Envigo, Placentia, CA) were used for SNI. Adult male and female Sprague-Dawley rats (56 days old, Charles River Laboratories, Raleigh, NC) were used for CION.

Mice: C57BL/6 mice were kept in light (12-h light: 12-h dark cycle; lights on at 07:00 h) and temperature (23 ± 3°C) controlled rooms. Male CD-1 mice (4 weeks) were used for sEPSC recordings in the spinal cord. Adult male and female C57BL/6J mice (8-12 weeks of age were used for the CFA (original mice were from Jackson and then bred at MSU with ad libitum access to food and water, group housed 3-4/cage) and for evaluating side effects and dose-response in the SNI-model (8 weeks of age, The Jackson Laboratory, JAX - Bar Harbor, ME USA). Adult male and female C57BL/6J mice (8–10 weeks of age, The Jackson Laboratory, JAX - Bar Harbor, ME USA) were used for CIPN.

Standard rodent chow and water were available *ad libitum.* All animal use was conducted in accordance with the National Institutes of Health guidelines, and the study was conducted in strict accordance with recommendations in the Guide for the Care and Use of Laboratory Animals of the College of Medicine at the University of Arizona, College of Osteopathic Medicine, New York University Grossman School of Medicine, Virginia Commonwealth University, Rutgers New Jersey Medical School, Michigan State University, and Rutgers School of Dental Medicine. All efforts were made to minimize animal suffering.

Biochemistry.

Dorsal root ganglion neuron cultures: Lumbar DRGs were dissected from 75-200 g female Sprague-Dawley rats using procedures as described previously (12). DRGs were excised and placed in sterile DMEM (Cat# 11965; Thermo Fisher Scientific, Waltham, MA). The ganglia were dissociated enzymatically with collagenase type I (5 mg/mL, Cat# LS004194; Worthington) and neutral protease (3.125 mg/mL, Cat# LS02104; Worthington, Lakewood, NJ) for 50 minutes at 37°C under gentle agitation. The dissociated cells were then centrifuged (800 rpm for 5 min) and resuspended in DMEM containing 1% penicillin/streptomycin sulfate (Cat# 15140, Life Technologies, Carlsbad, CA), 10% fetal bovine serum [HyClone]) and 30 ng/mL nerve growth factor (Cat# N2513, Millipore Sigma, St. Louis, MO). The cells were seeded on poly-D-lysine (0.1 mg/ml; Cat# P6407, Millipore Sigma, St. Louis, MO) and laminin (1

mg/ml; Cat#sc-29012, Santa Cruz Biotechnology, Dallas, TX) -coated 12- or 15-mm glass coverslips and incubated at 37°C. All cultures were used within 48 hours.

Immunocytochemistry and confocal microscopy: Immunocytochemistry was performed on female rat DRG neurons incubated with vehicle (0.1 % DMSO) or CBD3063 (20 µM) overnight. Cultured DRG neurons were fixed using ice-cold methanol for 5 min and then allowed to dry at room temperature. Fixed cells were rehydrated in PSB and then blocked with PBS containing 3% bovine serum albumin for 30 min at room temperature. Cell staining was performed with anti-$Ca_V2.2$ (Origene, Cat# TA308673, Rockville, MD) in PBS with 3% BSA overnight at 4°C. The cells were then washed thrice in PBS and incubated with PBS containing 3% BSA and secondary antibodies (Alexa 488 Chicken anti-Rabbit (Life Technologies, Carlsbad, CA)) for 1 h at room temperature. Coverslips were mounted and stored at 4°C until analysis. Immunofluorescent micrographs were acquired on a Leica SP8 inverted upright microscope using a 63X, oil immersion objective. For all quantitative comparisons among cells under differing experimental conditions, camera gain and other relevant settings were kept constant. The freeware image analysis program Image J (http://rsb.info.nih.gov/ij/) was used for quantifying cellular fluorescence. Regions of interest (i.e., cells) were defined by hand using Image J.

Calcium imaging: Changes in depolarization-induced calcium influx in rat DRG neurons were determined by loading neurons with 3 mM Fura-2AM for 30 minutes at 37°C (Cat# F1221; Thermo Fisher Scientific, Waltham, MA, stock solution prepared at 1 mM in DMSO, 0.02% pluronic acid, Cat# P-3000MP; Life Technologies, Carlsbad, CA) as previously described (13). DRG neurons were incubated overnight with 20 µM of test compounds. A standard bath solution containing 139 mM NaCl, 3 mM KCl, 0.8 mM $MgCl_2$, 1.8 mM $CaCl_2$, 10 mM Na-HEPES, 5 mM glucose, pH 7.4, was used. Depolarization was evoked with a 10 sec pulse of 90 mM KCl. Fluorescence imaging was achieved with an inverted microscope, Nikon EclipseTi-U (Nikon Instruments Inc., Melville, NY), using objective Nikon Fluor 4X and a Photometrics cooled CCD camera CoolSNAPES2 (Roper Scientific, Tucson, AZ) controlled by NIS Elements software (version 4.20, Nikon Instruments). The excitation light was delivered by a Lambda-LS system (Sutter Instruments, Novato, CA). The excitation filters (340 ± 5 nm and 380 ± 7 nm) were controlled by a Lambda 10 to 2 optical filter change (Sutter Instruments, Novato, CA). Fluorescence was recorded through a 505-nm dichroic mirror at 535 ± 25 nm. Images were taken every ~2.4 seconds during the time course of the experiment to minimize photobleaching and phototoxicity. To provide acceptable image quality, a minimal exposure time that provided acceptable image quality was used. Changes in $[Ca^{2+}]c$ were monitored following a ratio of F_{340}/F_{380}, calculated after subtracting the background from both channels.

In vivo calcium imaging (fiber photometry): Adult male and female wildtype mice received 500 nL of AAV9-CaMKIIa-GCamp6s-WPRE-SV40 (Addgene) in the right parabrachial nucleus (PBN) to transfect glutamatergic PBN neurons with the calcium indicator GCamp6s (coordinates: A/P-5.15 mm, M/L+/- 1.45 mm, D/V-3.45 mm). Virus was precisely administered with a Nanoject II Auto-Nanoliter Injector (Drummond) at a rate of 2 nL/sec and a wait time of 5 minutes to prevent backflow. Directly following viral infusion, a fiber optic cannula with black ceramic ferrule (RWD, 1.25 mm ferrule diameter, 200 µm core diameter, and 0.37 numerical aperture) was chronically implanted in the right PBN and fixed to the skull using dental cement (Cat# 10-000-786, Stoelting). Mice were allowed 21 days to recover before undergoing baseline testing. Mice were acclimated in acrylic boxes on wire mesh with fiber optic patch cord attached for at least one hour prior to testing. Calcium transients were collected continuously (FP3002, Neurophotometrics) during mechanical stimulation protocol. A 0.07 g von Frey filament, 1.0 g von Frey filament, or blunted thumbtack was applied perpendicularly to the outer plantar surface of the left hindpaw for approximately one second. Each stimulus was repeated three times with two minutes between stimuli. Using custom MatLab scripts the GCamp6s signal (470 nm laser) was normalized to the isosbestic control 405 nm laser signal. Area under the curve was calculated for the fifteen seconds directly following stimulus application and normalized to the average of the area under the curve for fifteen seconds directly before stimulus. The day after baseline recordings, animals underwent spared nerve injury surgery (SNI, described below) to induce neuropathic pain. Twenty-one days following SNI, the fiber photometry protocol was repeated in the same animals to collect post SNI responses of glutamatergic neurons in the PBN to mechanical stimuli. Two days later, the same fiber photometry protocol was conducted again 1-2 hours after intraperitoneal injection of either CBD3063 (10 mg/kg) or

gabapentin (30 mg/kg). Two days later, the behavior and recording paradigm was repeated in a cross over design so that each animal received both CBD3063 and gabapentin in a randomized order. Following the completion of the experiment, animals were transcardially perfused with ice cold 1x PBS and 10% neutral buffered formalin (Cat# SF98-4, Fisher Scientific) before brains were extracted for verification of viral infection and fiberoptic placement. Thirty µm thick coronal brain sections were obtained on a cryostat and stored at 4°C.

To visualize GCaMP6s expression we performed immunohistochemistry for GFP. Briefly, sections were washed 3 times in PBS for 5 minutes, incubated in normal goat serum (Cat# 5425, Cell Signaling Technology) based blocking buffer (PBS with 5% normal goat serum 0.1% Triton X-100) for one hour, and incubated in primary antibody (Rabbit anti-GFP 1:1000 in blocking buffer, Cat# AB3080, Millipore Sigma) overnight at room temperature on an orbital shaker. Sections were then washed 3 times in PBS with 0.1% Triton X-100 for 5 minutes, incubated for 1.5 hours in secondary antibody (goat anti rabbit AlexaFluor 488, Cat# A11008, Invitrogen), and washed again in PBS before being mounted on SuperFrost Plus microscope slides (Cat# 22-037-246, Fisher Scientific), coverslipped with Vectashield Plus antifade mounting medium with DAPI (H-2000-10, Vector Laboratories), and imaged at 20x on Leica DMi8 inverted widefield microscope. Three animals were excluded from the study due to fiberoptic headcap removal between baseline testing and post SNI testing. No animals were excluded due to post hoc target verification. Final n=8, 4 males and 4 females.

Proximity ligation assay: The proximity ligation assay (PLA) was performed as described previously (14-16) to visualize protein–protein interactions by microscopy. This assay is based on paired complementary oligonucleotide-labelled secondary antibodies that can hybridize and amplify a red fluorescent signal only when bound to two corresponding primary antibodies whose targets are in close proximity (within 30 nm). Briefly, female rat DRG neurons were fixed using ice-cold methanol for 5 minutes and allowed to dry at room temperature. The proximity ligation assay was performed according to the manufacturer's protocol using the Duolink Detection Kit with PLA PLUS and MINUS probes for mouse and rabbit antibodies (Duolink in situ detection reagents red, cat. no. DUO92008; Duolink in situ PLA probe anti-rabbit MINUS, cat. no. DUO92005; Duolink in situ PLA probe anti-mouse PLUS, cat. no. DUO92001, Sigma-Aldrich). Primary antibodies (1/1000 dilution) were incubated for 1 hour at RT; CaV2.2 (Cat# ACC-002; Alomone, RRID:AB_2039766) and CRMP2 (Cat#11096; Tecan, immunobiological lab, RRID:AB_494511). Cells were then stained with 49,6-diamidino-2-phenylindole (DAPI, 50 µg/mL) to detect cell nuclei and mounted in ProLong Diamond Antifade Mountant (Cat# P36961, Life Technologies Corporation). Immunofluorescent micrographs were acquired using a Plan-Apochromat 63x/1.4 oil CS2 objective on a Leica SP8 confocal microscope operated by the LAS X microscope software (Leica). Camera gain and other relevant settings were kept constant throughout imaging sessions. Image J was used to count the number of PLA puncta per cell.

Calcitonin gene-related peptide release: Adult female rats were anesthetized with 5% isofluorane and then decapitated. Two vertebral incisions (cervical and lumbar) were made to expose the spinal cord. Pressure was applied to a saline-filled syringe inserted into the lumbar vertebral foramen, and the spinal cord was extracted. Only the lumbar region of the spinal cord was used for the calcitonin gene-related peptide (CGRP) release assay. Baseline treatments involved bathing the spinal cord in standard Tyrode solution. The excitatory solution, consisting of 90 mM KCl, was paired with the treatment. These fractions (5 minutes, 700 µL each) were collected for measurement of CGRP release. Samples were immediately stored in a −20˚C freezer. CBD3063 (20 µM), or vehicle (0.1% DMSO) was added to the pretreatment (30 min) and cotreatment fractions. The concentration of CGRP released into the buffer was measured by enzyme-linked immunosorbent assay (Cat# 589001; Cayman Chemical, Ann Arbor, MI).

Electrophysiology.

Whole-cell patch-clamp recordings of Ca^{2+}, Na^{+}, K^{+} and HCN currents in acutely dissociated DRG neurons: Recordings were obtained from acutely dissociated DRG neurons obtained from female rats as described earlier (13). Patch-clamp recordings were performed at room temperature (22–24°C). Currents were recorded using an EPC 10 Amplifier-HEKA (HEKA Elektronik, Ludwigshafen, Germany) linked to a computer with Patchmaster software. DRG neurons were incubated overnight (~16-24 h) with 20 µM of CBD3063.

For total calcium current (I_{Ca2+}) recordings, the external solution consisted of the following (in mM): 110 N-methyl-D-glucamine, 10 $BaCl_2$, 30 TEA-Cl, 10 HEPES, 10 glucose, 0.001 TTX (pH 7.29 adjusted with TEA-OH, and mOsm/L= 310). Patch pipettes were filled with an internal solution containing (in mM): 150 $CsCl_2$, 10 HEPES, 5 Mg-ATP, and 5 BAPTA, (pH 7.24 adjusted with CsOH, and mOsm/L= 305). Peak Ca^{2+} current was acquired by applying 200-millisecond voltage steps from −70 to +60 mV in 10-mV increments from a holding potential of −90 mV to obtain the current-voltage (I-V) relation. To measure the different subtypes of Ca^{2+} channels, DRGs were treated with a Ca_V inhibitor cocktail omitting the inhibitor specific to the subtype being tested (e.g., to measure $Ca_V2.2$ currents, ω-conotoxin GVIA is omitted): Nifedipine (10 µM, L-type), ω-Conotoxin-GVIA (500 nM, P/Q-type) (17), SNX482 (200 nM, R-type) (18), ω-agatoxin (200 nM, P/Q-type) (19), TTA-P2 (1 µM, T-type) (20).

For Na^+ current (I_{Na+}) recordings, the external solution contained (in mM): 130 NaCl, 3 KCl, 30 tetraethylammonium chloride, 1 $CaCl_2$, 0.5 $CdCl_2$, 1 $MgCl_2$, 10 D-glucose and 10 HEPES (pH 7.3 adjusted with NaOH, and mOsm/L= 324). Patch pipettes were filled with an internal solution containing (in mM): 140 CsF, 1.1Cs-EGTA, 10 NaCl, and 15 HEPES (pH 7.3 adjusted with CsOH, and mOsm/L= 311). Peak Na^+ current was acquired by applying 150-millisecond voltage steps from −70 to +60 mV in 5-mV increments from a holding potential of −60 mV to obtain the current-voltage (I-V) relation.

To isolate potassium currents (I_{K+}), DRG neurons were bathed in external solution composed of (in millimolar): 140 N-methyl-glucamine chloride, 5 KCl, 1 $MgCl_2$, 2 $CaCl_2$, 10 D-glucose and 10 HEPES (pH adjusted to 7.3 with KOH and mOsm/L= 313). Recording pipettes were filled with internal solution containing (in mM): 140 KCl, 2.5 $MgCl_2$, 4 Mg-ATP, 0.3 Na-GTP, 2.5 $CaCl_2$, 5 EGTA, and 10 HEPES (pH adjusted to 7.3 with KOH and mOsm/L= 320). From a holding potential of -60 mV, total I_K activation was determined by applying 300-millisecond voltage steps from −80 to +60 mV in 10-mV increments. To obtain I_{KA} a 4-s pre-pulse to −100 mV was applied followed by voltage steps of 500 milliseconds that ranged from −80 to +40 mV in +20-mV increments at 15-s intervals. I_{KS} was obtained from a conditioning 4-sec pre-pulse to −40 mV followed by voltage steps of 500 milliseconds that ranged from −80 to +40 mV in +20-mV increments at 15-s intervals.

To isolate HCN currents, the external solution consisted of the following (in mM): 40 NaCl, 4 KCl, 1.8 $CaCl_2$, 1 $MgCl_2$, 10 D-glucose and 1 HEPES (pH adjusted to 7.4 with NaOH and mOsm/L= 298). Internal solution consisted of the following (in mM): 140 KCl, 2.5 Mg-ATP, 0.5 Na-GTP, 2 EGTA, 10 HEPES and 0.0001 cAMP (pH adjusted to 7.4 with KOH and mOsm/L= 310). From a holding potential of -60 mV HCN activation was determined by applying 5000-millisecond voltage steps from −130 to -40 mV in 10-mV increments.

Normalization of currents to each cell's capacitance (pF) was performed to allow for collection of current density data. For I-V curves, functions were fitted to data using a non-linear least squares analysis. I-V curves were fitted using double Boltzmann functions:

$$f = a + g1/(1+\exp((x-V_{1/2}1)/k1)) + g2/(1+\exp(-(x-V_{1/2}2)/k2))$$

where x is the pre-pulse potential, $V_{1/2}$ is the mid-point potential and k is the corresponding slope factor for single Boltzmann functions. Double Boltzmann fits were used to describe the shape of the curve, not to imply the existence of separate channel populations. Numbers *1* and *2* simply indicate first and second mid-points; *a* along with *g* are fitting parameters.

Activation curves were obtained from the I-V curves by dividing the peak current at each depolarizing step by the driving force according to the equation: $G = I/(V_{mem}-E_{rev})$, where I is the peak current, V_{mem} is the membrane potential and E_{rev} is the reversal potential. The conductance (G) was normalized against the maximum conductance (G_{max}). For total and the different subtypes of Ca^{2+} currents, steady-state inactivation (SSI) curves were obtained by applying an H-infinity protocol that consisted of 1.5-seconds conditioning pre-pulses from −100 to +30 mV in 10-mV increments followed by a 20-millisecond test pulse to +10 mV. For Na^+ currents, SSI curves were obtained by applying an H-infinity protocol that consisted of

1-second conditioning pre-pulses from −120 to +10 mV in 10-mV increments followed by a 200-millisecond test pulse to +10 mV. Inactivation curves were obtained by dividing the peak current recorded at the test pulse by the maximum current (I_{max}). Activation and SSI curves were fitted with the Boltzmann equation.

Action potential recordings in acutely dissociated DRG neurons: For current-clamp recordings the external solution contained (in millimolar): 154 NaCl, 5.6 KCl, 2 $CaCl_2$, 1 $MgCl_2$, 10 D-Glucose, and 8 HEPES (pH 7.4 adjusted with NaOH, and mOsm/L= 300). The internal solution was composed of (in millimolar): 137 KCl, 10 NaCl, 1 $MgCl_2$, 1 EGTA, and 10 HEPES (pH 7.3 adjusted with KOH, and mOsm/L= 277). At room temperature (22–24°C), whole-cell patch clamp configuration was made, and current-clamp mode was performed to record action potentials. DRG neurons with a resting membrane potential (RMP) more hyperpolarized than −40 mV, stable baseline recordings, and evoked spikes that overshot 0 mV were used for experiments and analysis. The action potentials were evoked by current injection steps from 0–120 pA with an increment of 10 pA in 300 ms. Rheobase was measured by injecting currents from 0 pA with an increment of 10 pA in 50 ms. Analyses were performed by using Fitmaster software (HEKA) and Origin 9.0 software (OriginLab).

Whole-cell patch clamp recordings of spinal cord slices: Spinal cord slices were prepared from male CD-1 mice (4 weeks) as we described previously (21). Briefly, the vertebral column was isolated and immersed in ice-cold oxygenated N-methyl-D-glucamine (NMDG)-based artificial CSF (ACSF) containing the following (in mM): 93 NMDG, 93 HCl, 30 $NaHCO_3$, 20 HEPES, 2.5 KCl, 1.2 NaH_2PO_4, 10 $MgCl_2$, 0.5 $CaCl_2$, 25 glucose (osmolality, 305–310 mmol/kg). The lumber spinal cord was removed and glued onto the cutting platform with the adhesive Loctite 404 (Loctite). Transverse spinal cord slices (300 μm) were cut in NMDG ACSF with a Compresstome VF-200 slicer (Precisionary Instruments Inc., Greenville, NC, USA), then immediately transferred to a holding chamber and incubated in the oxygenated normal ACSF containing (in mM): 26 $NaHCO_3$, 120 NaCl, 5 KCl, 1.25 NaH_2PO_4, 1 $MgCl_2$, 1 $CaCl_2$, 12.5 glucose (osmolality, 305–310 mmol/kg) for 1 h at 32 °C, then maintained in oxygenated ACSF at room temperature (24–25 °C). A single slice was transferred to a submersion-type recording chamber and mechanically stabilized with a platinum ring.

Spinal cord neurons in lamina I or II were visualized using an infrared differential contrast and fluorescence microscopy (Leica Microsystems). Excitatory postsynaptic currents (EPSC) were recorded with an Axon 700B amplifiers, a Digidata 1440A A/D converter, and Clampfit 10.4 software (Molecular Devices Co., Union City, CA, USA). Data were filtered at 2 kHz and sampled at 5 kHz. Throughout the experiments, slices were perfused continuously with warm (37 °C) oxygenated ACSF (2-3 mL/min). Patch pipettes (6–8 MΩ) were filled with the internal solution (in mM) 140 cesium methanesulfonate, 5 KCl, 2 $MgCl_2$, 10 HEPES, 2 MgATP, 0.2 GTP for recordings under voltage-clamp. The excitatory postsynaptic currents (EPSCs) were recorded at a holding potential of -60 mV in the presence of gabazine (10 μM), SCH50911 (20 μM), and strychnine (0.5 μM), which block $GABA_A$, $GABA_B$ and glycine receptors, respectively. These events were blocked by DNQX (20 μM), an antagonist of α-amino-3-hydroxy-5-methylisoxazole-4-propionic acid (AMPA) receptors, indicating that they were mediated by AMPA receptors.

Pain models.

Spared nerve injury (SNI) model of neuropathic pain:
Mice and rats were anesthetized with isoflurane (5% induction, 2% maintenance in 2 L/min air), and skin on the lateral surface of the left hind thigh was incised. Then, the biceps femoris muscle was dissected to expose the three terminal branches of the sciatic nerve. The common peroneal and tibial branches were tightly ligated with 4-0 silk and axotomized 2.0 mm distal to the ligation. In rats, the closure of the incision was made in two layers. The muscle was sutured once with 5-0 absorbable suture; skin was autoclipped. Animals were allowed to recover for 10 days before any testing. On the 10th day after SNI, CBD3063 (0.3 μg/kg) or 1% DMSO was injected intrathecally. Mechanical allodynia was assessed 10 days after surgery. In mice, the skin was autoclipped. Twenty-one days after surgery, mice were injected i.p. wih vehicle (10% DMSO in saline), CBD3063 (0.01, 0.10, 1.0 and 10 μg/kg) or gabapentin (GBP; 30 mg/kg) and mechanical and cold allodynia were assessed.

Chemotherapy induced peripheral neuropathy (CIPN) model of paclitaxel: Paclitaxel was purchased from VCU Health Pharmacy (Athenex, NDC 70860-200-50, Richmond, VA, USA) and dissolved in a 1:1:18 mixture of 200 proof ethanol, kolliphor, and distilled water (Sigma-Aldrich) to a dose of 8 mg/kg. Paclitaxel was then administered intraperitonially every other day for four doses to 8 males and 8 females. The remaining 16 animals received the vehicle 1:1:18 at a volume of 10 ml/kg, i.p. following the same injection regimen. After the final Paclitaxel and 1:1:18 injection, these two groups were separated further whereby 4 males and 4 females from each group for compound-treatment (n = 8/group) (22).

Mechanical and cold sensitivity baselines (BL) were measured before induction of the pain model. Mice were then injected with paclitaxel (8 mg/kg, i.p. every other day for a total of 4 doses) or vehicle as explained above and tested at day 21 after the first dose of paclitaxel (time 0). Mice were then injected i.p. with CBD3063 (9 mg/kg) or 10% DMSO (vehicle) and then tested for mechanical and cold sensitivity at the following time points: 1, 3, 6 and 24 hr.

Chronic constriction injury of the rat's infraorbital nerve: Prior to surgical procedures, male rats were anesthetized with intraperitoneal injections of ketamine (50 mg/kg)/xylazine (7.5 mg/kg) solution. A single investigator performed the surgeries to minimize variability. Unilateral chronic constriction injury to the infraorbital nerve (CION) was used to induce trigeminal neuropathic pain in rats as previously described (23). Briefly, following anesthesia, an approximately 1 cm long incision was made along the left gingivobuccal sulcus beginning just proximal to the first molar. ION was exposed (~0.5 cm) and freed from the surrounding tissue. Two chromic gut (4-0) ligatures were loosely tied around the exposed nerve. The incision was closed with the absorbable sutures.

Complete Freund's adjuvant (CFA)-induced peripheral inflammation: Peripheral inflammation was induced by administration of 5 µg Complete Freund's adjuvant (1 mg/ml, each ml of CFA contains 1 mg of heat-killed and dried Mycobacterium tuberculosis). Two days post-CFA injection, mechanical hypersensitivity was measured again followed by a single CDB3063 injection administrated intraplantarly in the inflamed paw (25 µg in 5 µL) or saline as vehicle.

Compound administration.

Intraperitoneal: Naïve male and female mice were subjected to intraperitoneal administrations of CBD3063 (10 mg/kg), gabapentin (30 mg/kg), or vehicle (10% DMSO; 1 ml/kg). Intraperitoneal delivery was carried out using a 30-gauge, 0.3-inch needle, inserted into the lower left quadrant of the abdomen. The needle was positioned parallel to the backbone at a 45° angle to the abdominal wall. Behavioral assessments were conducted at 1-, 2-, 3-, 4-, 5-, and 6-hours following administration to measure paw withdrawal threshold and cold aversion time. Additionally, assessments for hotplate, tail flick, tail suspension, open field, and novel object recognition were performed 2 h post-administration.

Intranasal: At 22 days post-CION, half of the rats received an intranasal CBD3063 (200 µg in 20µL isotonic saline) and the remaining half received 20µL of isotonic saline (vehicle-control). Intranasal delivery was performed with a pipette and a disposable plastic tip. Immediately after administration, the head of the animal was held in a tilted back position for ~15 seconds to prevent loss of solution from the nare. Behavioral assessments were done at 30 minutes, 1-, 2-, and 3-hours post-administration.

Intraplantar: To establish the inflammatory pain model, naïve mice were subjected to an intraplantar injection of CFA (5 µg per paw. 1 mg/ml, each ml of CFA contains 1 mg of heat-killed and dried Mycobacterium tuberculosis). Intraplantar delivery was carried out using a 30-gauge, 0.3-inch needle, inserted subcutaneously into the center of the hind foot forming a small bleb at the injection site. Two days after CFA injection, male and female mice received an ipsilateral intraplantar administration of CBD3063 (25 µg/5 µl) or vehicle (saline) and the paw withdrawal threshold were measured at 1-, 2-, 3-, and 4-hours following administration.

Indwelling intrathecal catheter: Rats were anesthetized with ketamine/xylazine 80/12 mg/kg intraperitoneally (i.p.) (Sigma-Aldrich, St. Louis, MO), and their head was placed in a stereotaxic frame. The cisterna magna was exposed and incised. As previously reported, an 8-cm catheter (PE-10; Stoelting, Wood Dale, IL) was implanted, terminating in the lumbar region of the spinal cord (24).

Catheters were sutured (using 3–0 silk sutures) into the deep muscle and externalized at the back of the neck. Autoclips were used to close the skin, and other surgeries were performed after a 5- to 7-day recovery period. A single intrathecal administration of CBD3063 (0.3 µg/kg), was performed seven days following SNI. To assess the long-term antinociceptive effects of CBD3063, rats were injected with CBD3063 (0.3 µg/kg) starting 7 days after SNI surgery and once a day for 14 days.

Behavioral testing.

Mechanical sensitivity test:

Rats with SNI. Mechanical allodynia was assessed by measuring rats' paw withdrawal threshold in response to probing with a series of fine calibrated filaments (von Frey, Stoelting, Wood Dale, IL). Rats were placed in suspended plastic cages with wire mesh floor, and each von Frey filament was applied perpendicularly to the plantar surface of the paw. The "up-and-down" method (sequential increase and decrease of the stimulus strength) was used to determine the withdrawal threshold Dixon's nonparametric method was used for data analysis, as described by Chaplan et al (25). Data were expressed as the mean withdrawal threshold.

Rats with CION. von Frey detection threshold was measured by applying von Frey monofilaments delivering calibrated amount of force ranging from 0.0008 g to 1 g or converted to log units 1.65 to 4.08 (EXACTA Precision & Performance monofilaments, Stoelting) within the ION dermatome in ascending order of intensity (26). The lowest filament that evoked one withdrawal response was designated as the withdrawal threshold. A decrease in the withdrawal threshold is indicative of development of hypersensitivity.

Mice. Animals were placed in acrylic cages on a mesh grid floor and allowed to acclimate for 60 minutes before the experiment. A Von Frey filament was applied perpendicularly to the plantar surface of the paw to determine the 50% paw withdrawal threshold using the up-down method as previously described (25). In sham animals, a value of 0.8-1 g was considered normal, while the presence of tactile allodynia was considered when the 50% withdrawal threshold of the limb was < 0.2 g.

Cold sensitivity test: Mice were individually caged on mesh metal flooring for 30 minutes prior to testing. 20 µL of acetone (Sigma-Aldrich, MO, USA) was applied onto the lateral side of the plantar surface of each hind paw via pipette or a syringe connected to PE-90 tubing. The cumulative time spent licking, slapping, flinching, or shaking the hind paw was recorded for 60 seconds.

Tail-Flick test: For this test, mice were injected with CBD3063 (10 mg/kg; i.p.), gabapentin (30 mg/kg) or vehicle (1 ml/kg, DMSO 10%, i.p.) and 2 hours later the tail flick test was performed as previously reported (1). Mice were immobilized and the distal third of the tail was gently immersed in warm water at a temperature of 52°C. The duration until tail withdrawal from the water (tail withdrawal latency) was recorded, considering a 10-second cut-off to avoid tissue damage.

Hot plate test: The hot plate test was performed as previously reported (1). Mice received a single intraperitoneal administration of CBD3063 (10 mg/kg), gabapentin (30 mg/kg) or vehicle (1 ml/kg, DMSO 10%, i.p.) and 2 hours post-administration each mouse was placed on a heated metal plate (Hot/Cold Plate, Ugo Basile) maintained at 52 ± 2 °C, without prior habituation. The onset of the first nocifensive response was recorded, (i.e., hind paw flinching, paw licking, or jumping). A 30-second cut-off was established to prevent potential tissue damage.

Open field test (OFT): OFT experiments were conducted in mice 2h after i.p. injection of CBD3063 (10mg/kg), gabapentin (30mg/kg) and vehicle (10% DMSO in saline). Doses and timing were chosen based on the dose-response results showing similar analgesic effects of the two compounds at those doses. The OFT apparatus was a squared arena (30*30cm), and each animal was recorded for 15 minutes using an overhead camera (Microsoft LifeCam HD-3000) and tracking of the center-point was performed using ANY-maze software (version 7.2, Stoelting Co). The arena was divided into center (15*15 cm) and peripheral (7.5 cm along the perimeter) zones. The duration of time spent in the peripheral versus center zones of the arena was used as a marker for anxiety-like behavior, while "time immobile" was used to assess sedative-like effects.

Tail suspension test: The tail suspension test was carried out as previously described (27). In brief, mice received CBD3063 (10 mg/kg; i.p.), gabapentin (30 mg/kg; i.p.) or vehicle (1 ml/kg, DMSO 10%, i.p.) and 2 hours post-administration the mice were gently handled, and a climb-stopper was attached to their tail. Then the animals were suspended by their tails using adhesive tape and monitored over a 6-minute period. The immobility time was determined by analyzing the mobility time (i.e., strong shaking of the body, movement of the limbs like running, climb-type movements), which was subtracted from the total time of test.

Novel object recognition (NOR): The NOR test was performed similarly to previously described (28), with some modifications. Testing was carried out in the same squared arena as the OFT test, 3-5 days following the OFT, making the OFT-test also serve as habituation to the arena without objects. A camera was positioned directly above the arena and connected to a computer performing live-tracking and recording of the behavior using ANY-maze software, with tracking of nose and center points. The familiar/similar objects were brown circular glass bottles (d; 7 cm, h; 18 cm), while the "novel" object was a translucent elliptical glass bottle (d; 8*4 cm, h; 15 cm) containing white powder for coloring. The animal was placed in the arena facing away from the objects, and first allowed 10minutes freely exploration and familiarization to the arena including the two similar brown glass bottles (making these "familiar object" following the habituation phase), placed in two opposite quadrants of the arena.

Injections of CBD3063 (10mg/kg), gabapentin (30mg/kg) and vehicle (10% DMSO in saline) were performed i.p. 1 h after the familiarization, and 2 h before the test-session. For the test-session, the animal was reintroduced to the arena for a 5min test, where one of the familiar objects had been replaced with the novel object. The object replaced / side was alternated between test subjects and experimental groups to randomize for potential side-preferences in the arena. Exploration of an object was defined as the nose being within 2cm of the objects while facing them, and upon completion, all recordings/trackings were corrected for appropriate nose-tracking and exploration. The proportion of time spent exploring the objects were assessed by calculating a proportion of time exploring the novel object, using the following calculation The proportion of time spent exploring the objects were assessed by calculating a proportion of time exploring the novel object, using the following calculation from Ferdousi et al (29).

$$Discrimination\ index = \frac{\text{Time spent exploring novel} - \text{familiar object}}{\text{Time spent exploring novel} + \text{familiar onject}}$$

Pinprick assay: Pinprick response score was measured by scoring the response to stimulation with a blunted acupuncture needle applied within the vibrissal pad od the rats. The scores were assigned as follows: 0=no response, 1=non-aversive response, 2=mild aversive response, 3=strong aversive response, 4=prolonged aversive behavior (30, 31). An increase in the response score is indicative of development of hypersensitivity.

Locomotor activity: Mice were placed into individual photocell activity cages (28 x 16.5 cm; Omnitech, Columbus, OH) 60 min after i.p. saline or CBD3063 (9 mg/kg) administration (n=8/group; 50% male and 50% female). Interruptions of the photocell beams (two banks of eight cells each) were then recorded for the next 60 min. Data were measured as the average number of photocell interruptions during the 60 min test period.

Pharmacokinetics of CBD3063 in mice. The pharmacokinetics (PK) analysis of CBD3063 in mice was conducted by WuXi Apptec (Lab Testing Division, Cranbury NJ, USA). Three male C57BL/6 mice were injected intraperitoneally with a single dose of 9 mg/kg of CBD3063, and plasma samples were collected at 0.25, 0.5, 1, 2, 4, 8, and 24 hour post dosing time points. Briefly, blood samples (~30 µL) were collected into sample tubes and kept on ice, then plasma was extracted by centrifugation at 4°C, 3000g for 5 min. Plasma was promptly frozen on dry ice and stored at -70 ± 10 °C until analysis by LC-MS/MS. An aliquot of 20 µL sample was protein precipitated with 200 µL IS solution, the mixture was vortex-mixed well and centrifuged at 4000 rpm for 10 min, 4℃. An aliquot of 100 µL supernatant was transferred to sample plate, 100 µL H2O was added to each supernatant, then the plate was shake at 800 rpm for 10

min. 2 µL supernatant was then injected for LC-MS/MS analysis. A calibration curve of 1-3000ng/mL for CBD3063 in blank mouse plasma and a set of QC samples consisting of low, middle and high concentrations were applied for the LC-MS/MS method. The pharmacokinetics of CBD3063 was analyzed using Phoenix WinNonlin software (version 8.3) and non-compartmental analysis model. The half-life ($t_{1/2}$) was calculated from a log-linear plot of concentration versus time.

Data Analysis. Graphing and statistical analysis were performed with GraphPad Prism (Version 9), and in IBM SPSS for the ANCOVA. All data sets were checked for normality using D'Agostino & Pearson test. Details of statistical tests, significance and sample sizes are reported in the appropriate figure legends. All data plotted represent mean ± SEM.

-For western blot experiments, statistical differences between groups were determined by Mann-Whitney test. Statistical significance of confocal imaging data was evaluated by Mann-Whitney test.

-For Ca^{2+} imaging experiments, data was analyzed by One-way ANOVA.

-For electrophysiological recordings: Normalized peak currents were analyzed by Kruskal-Wallis test followed by the Dunn's post hoc test; the significance of the I-V curves was analyzed by multiple Mann-Whitney tests; peak current density as well as $V_{1/2}$ midpoint potential and *k* slope factor were compared using Mann-Whitney test. For resting membrane potential and rheobase, the significance was analyzed by Mann-Whitney test; the significance of the number of evoked action potentials per step was analyzed by multiple Mann-Whitney tests; sEPSC frequency and amplitude were analyzed by paired t-tests; and cumulative probability by Kolmogorov-Smirnov test. iCGRP release was analyzed by 2-way ANOVA followed by Sidak's multiple comparisons test.

-Mice: For behavioral data were male and female data are combined, 2-way ANOVA followed by Tukey post-hoc test did not show any significant sex's effect for the outcome measures. When male and female data are separated, results were also compared using two-way ANOVA with time and treatment, as factors and Tukey post-hoc test. AUC were analyzed by One-way ANOVA followed by Tukey or Dunnett post-hoc tests, in addition to Two-Way ANOVA (treatment*sex) to assess sex-differences. An additional ANCOVA (treatment*sex, covariate; immobility) analysis was performed in SPSS for the NOR-data, to assess the potential confounding effects of immobility on the outcome.

Assessment of sex differences in CBD3063's efficacy: We found overall significant effects of sex on outcome measures like naïve cold aversion (**Fig. 6E**), thermal response latency (**Fig. 6F**), immobility in the Tail Suspension Test (**Fig. 6I**), and cold allodynia after SNI (**Fig. 5I**), but only for tail-flick assay (**Fig. 6C**) was there a sex*treatment interaction as GBP had greater effects in males than females. This suggests that despite sex-differences in general thresholds or response latencies, effects of CDB3063 treatment were similar for both males and females. Sex was found to have no statistical influence on the treatment-effects of CBD3063 in SNI-, paclitaxel- or CFA- induced injury, and for simplicity these datasets are presented combined across the genders (see **Dataset 1** for full statistics).

-Rats: Behavioral data was analyzed by Multiple Mann-Whitney tests or two-way ANOVA with time and treatment, as factors and Bonferroni post-hoc test were performed.

Detailed statistical analyses are presented in **Dataset 1**.

SI Figures and Legends.

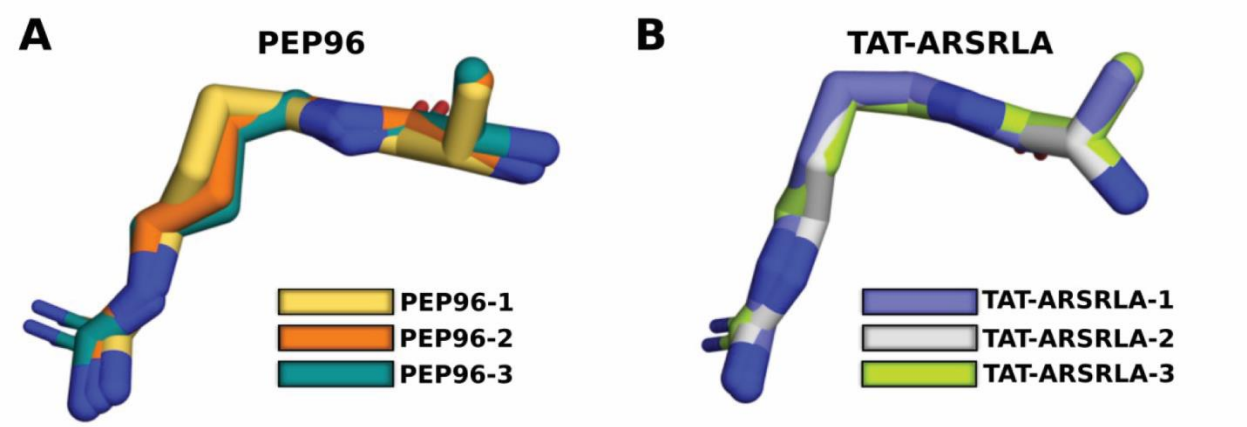

Figure S1. **Cluster centers for three independent simulations of the PEP96 and TAT-ARSRLA.** The clusters are based on (A) A_1R_2 (PEP96) and (B) $A_{12}R_{13}$ (TAT-ARSRLA) with less than 1 Å from cluster center.

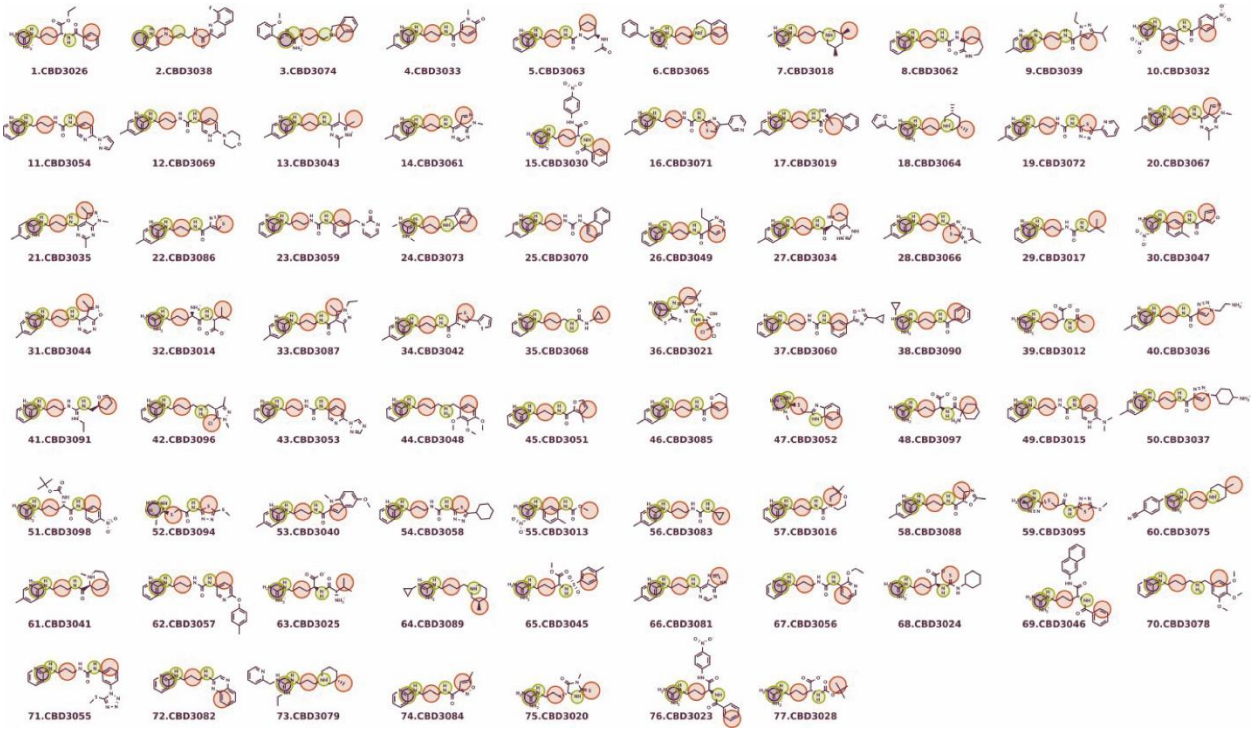

Figure S2. Full list of structures tested.

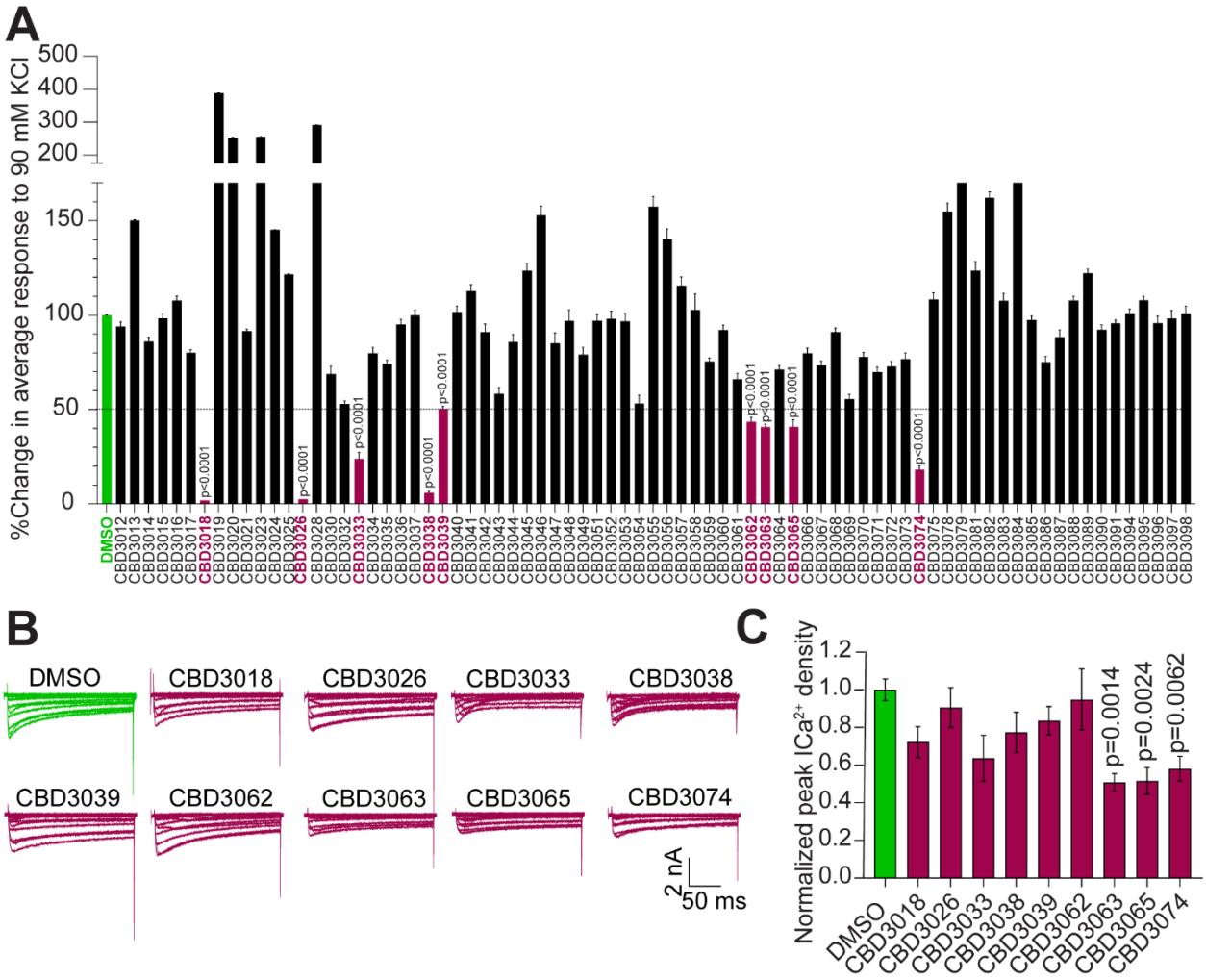

Figure S3. Compound screening using depolarization-induced Ca^{2+} influx and whole-cell patch-clamp in DRG neurons identify various high-voltage-activated Ca^{2+} channels inhibitors. (A) Percent change in average response of DRG sensory neurons incubated overnight with 20 µM of the indicated compounds in response to 90 mM KCl. n=61-629 cells; error bars indicate mean ± SEM. *p* values as indicated; One-Way ANOVA with the Dunnett post hoc test. Only the significances for the compounds that inhibit Ca^{2+} influx more than 50% are shown in the plot. (B) Representative calcium current traces recorded from small– to medium–sized DRGs incubated overnight with 0.1% DMSO or 20 µM of test compounds as indicated in the figure. Currents were evoked by 200-ms pulse between −70 and +60 mV. (C) Summary of bar graph showing the normalized peak total ICa^{2+} density. CBD3063, 3065 and 3074 significantly decreased total Ca^{2+} currents. n=16-98 cells (indicated in parenthesis) from seven separate rats; error bars indicate mean ± SEM; *p* values as indicated; Kruskal-Wallis test followed by Dunn's post hoc test. See **Dataset 1** for full statistics.

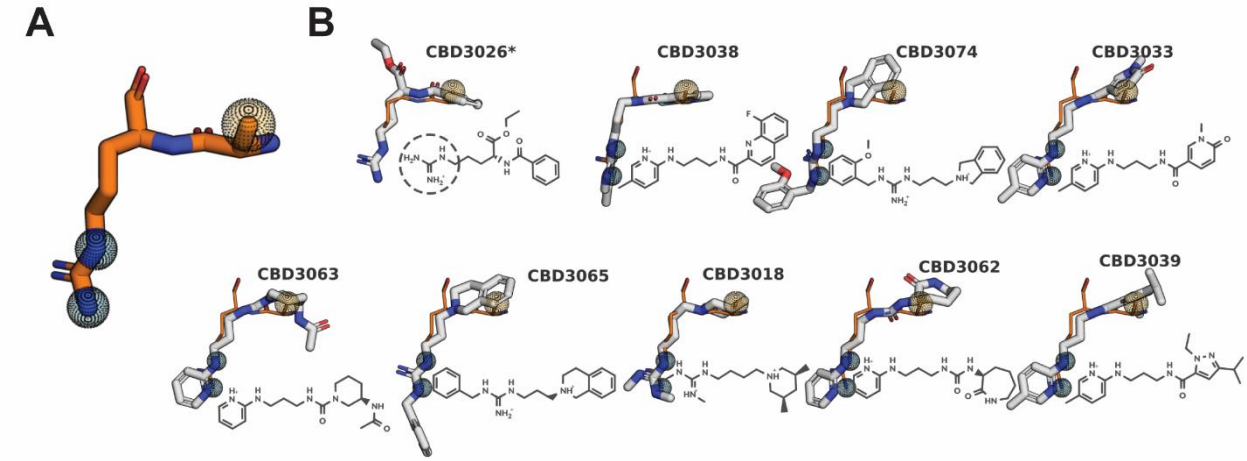

Figure S4. Shared chemotypes. (A) A_1R_2 cluster center highlighting three pharmacophores present in all compounds except CBD3026*. (B) Structures of compounds obtained from the ZincPharmer screen which were found to inhibit Ca^{2+} influx by more than 50% (**Fig. S3**). Dashed circle shows guanidine group (arginine).

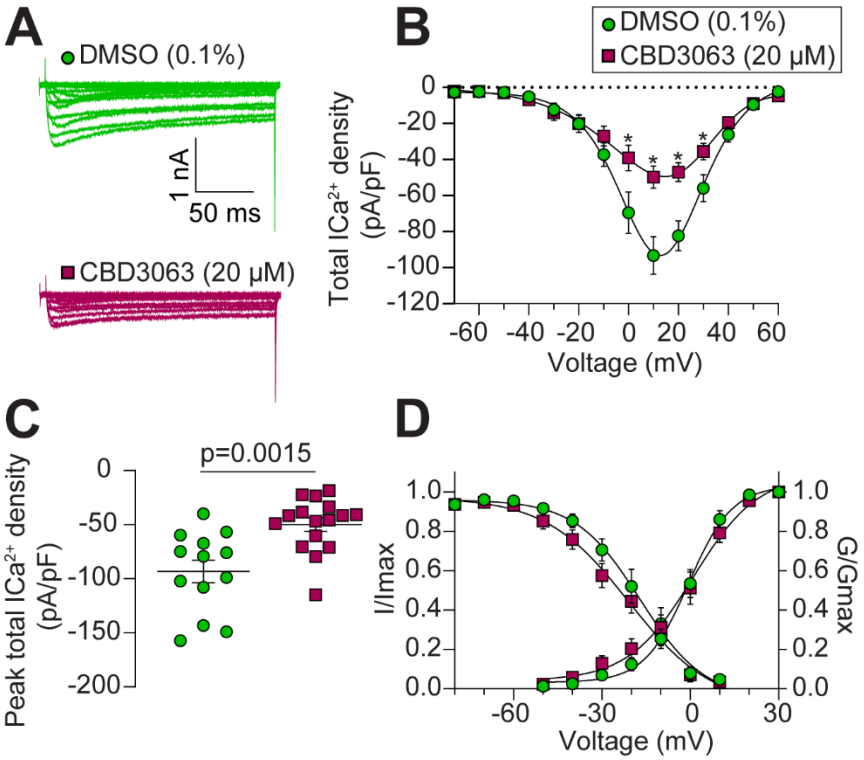

Figure S5. CBD3063 reduces total calcium currents in DRG neurons. (A) Representative calcium current traces recorded from small– to medium–sized DRGs incubated overnight with 20 µM of CBD3063 as indicated in the figure. Currents were evoked by 200-ms pulse between −70 and +60 mV. (B) Double Boltzmann fits for current density–voltage curve. Asterisk (*) indicate $p<0.05$; Multiple Mann-Whitney tests. (C) Summary of bar graph showing peak calcium current densities (pA/pF). CBD3063 decreased total Ca^{2+} current density. *p* value as indicated; Mann-Whitney test. (D) Boltzmann fits for voltage-dependent activation and inactivation as shown. Half-maximal activation potential of activation and inactivation ($V_{1/2}$) and slope values (*k*) for activation and inactivation are presented in **Table S2**. n=13-16 cells from four separate rats; error bars indicate mean ± SEM. See **Dataset 1** for full statistics.

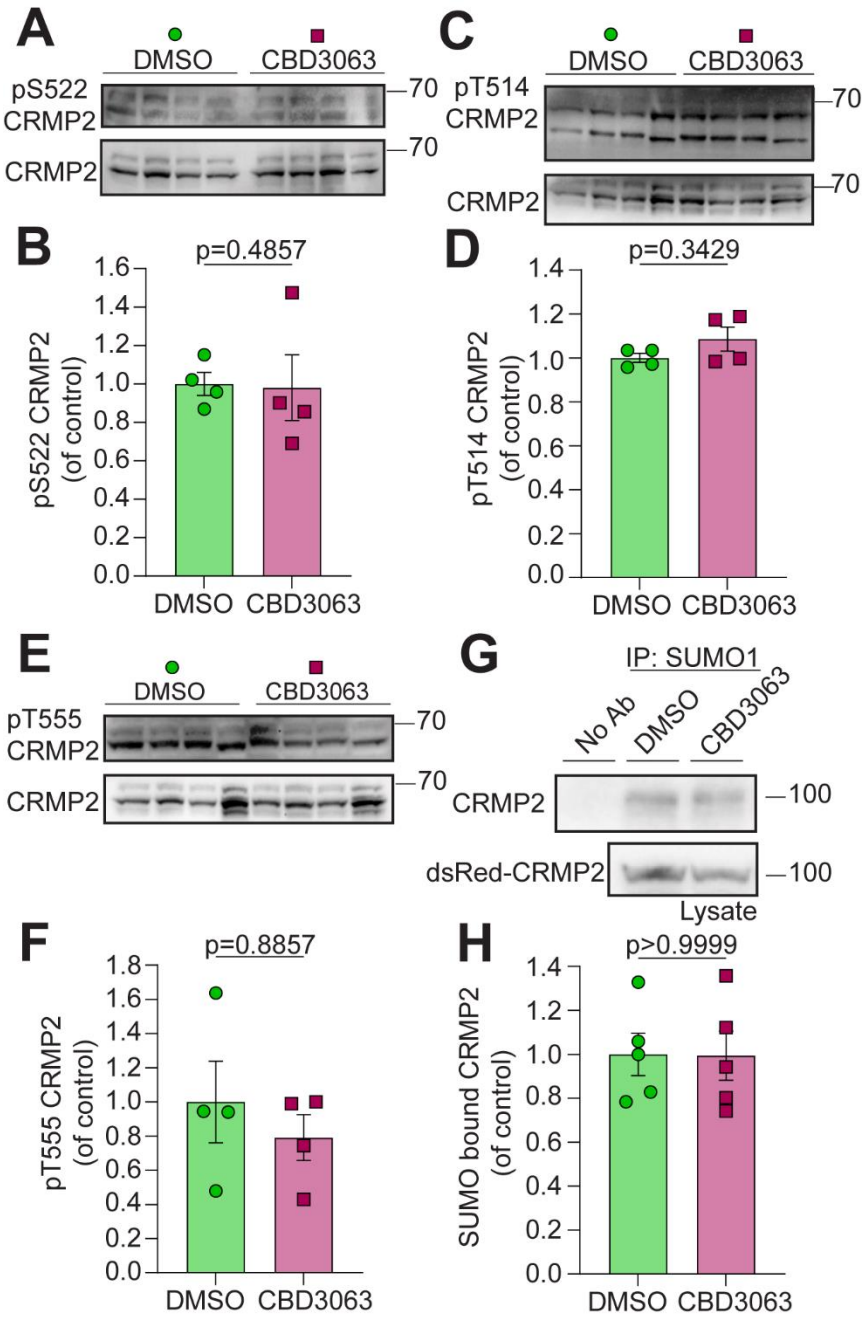

Figure S6. CBD3063 does not affect CRMP2 phosphorylation nor SUMOylation. Representative immunoblots (A, C and E) and quantitative analysis (B, D and F) of total and phosphorylated CRMP2 at the indicated kinase target sites from CAD cells treated overnight with 0.1% DMSO (as control) or 20 µM CBD3063 (n= 4 independent assays). Representative immunoblots (G) and summary (H) of SUMOylated CRMP2 from CAD cells transfected with dsRed-CRMP2 plasmid and treated overnight with 0.1% DMSO or 20 µM CBD3063 (n= 5 independent assays). Error bars show mean ± SEM; *p* values as indicated; Mann-Whitney test.

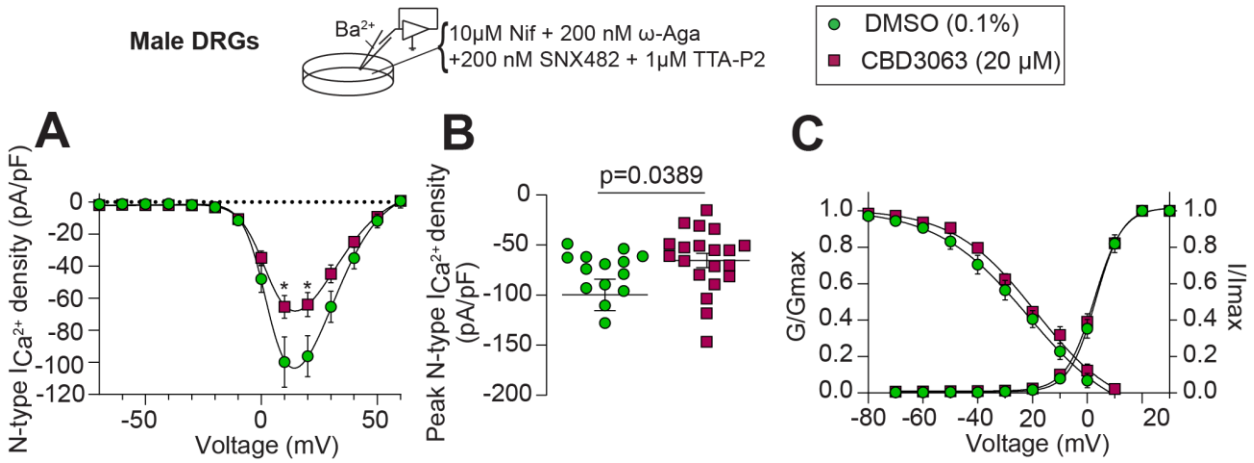

Figure S7. CBD3063 inhibits N-type calcium currents in male DRG neurons. *Top*: schematic showing composition of bath solution used to isolate N-type currents. (A) Double Boltzmann fits for current density–voltage curve of N-type calcium currents recorded from small– to medium–sized DRGs incubated overnight with 20 μM of CBD3063. Asterisks denote *p* values of less than 0.05; Mann-Whitney test. (B) Summary of bar graph showing peak calcium current densities (pA/pF). CBD3063 reduced $Ca_V2.2$ Ca^{2+} current density. *p* values indicated; Mann-Whitney test. (C) Boltzmann fits for voltage-dependent activation and inactivation as shown. Half-maximal activation potential of activation and inactivation ($V_{1/2}$) and slope values (*k*) for activation and inactivation are presented in **Table S2**. n=14-21 cells from three separate rats; error bars indicate mean ± SEM. See **Dataset 1** for full statistics.

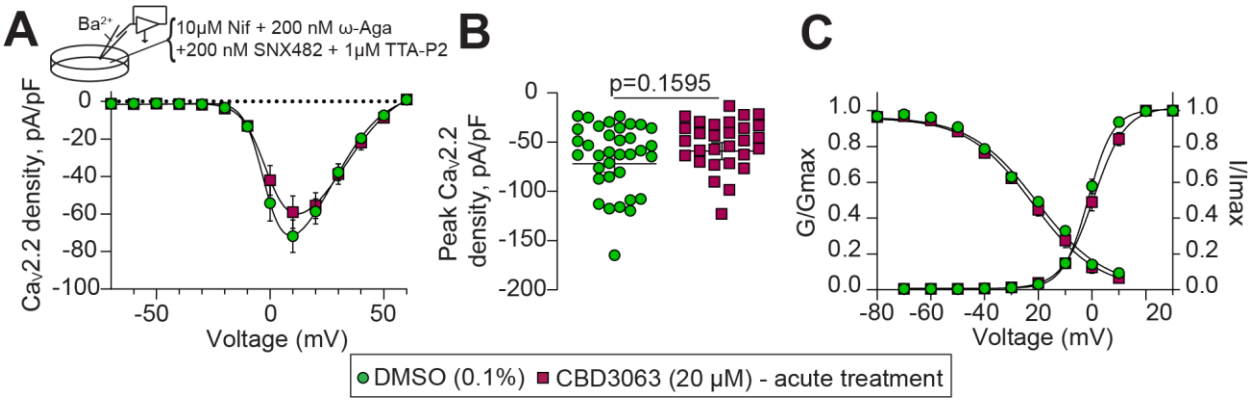

Figure S8. Acute application (15 min) of CBD3063 does not affect N-type calcium currents in DRG neurons. (A) *Top*: composition of bath solution used to isolate N-type currents. *Bottom*: Double Boltzmann fits for current density–voltage curve of N-type calcium currents recorded from small– to medium–sized DRGs incubated 15 minutes with 20 µM of CBD3063 as indicated in the figure. No statistical significance was observed after applying a Multiple Mann-Whitney tests. (B) Summary of bar graph showing peak calcium current densities (pA/pF). CBD3063 did not affect $Ca_V2.2$ Ca^{2+} current density. *p* value as indicated; Mann-Whitney test. (C) Boltzmann fits for voltage-dependent activation and inactivation as shown. Half-maximal activation potential of activation and inactivation ($V_{1/2}$) and slope values (*k*) for activation and inactivation are presented in **Table S2**. n=30-36 cells from three separate rats; error bars indicate mean ± SEM. See **Dataset 1** for full statistics.

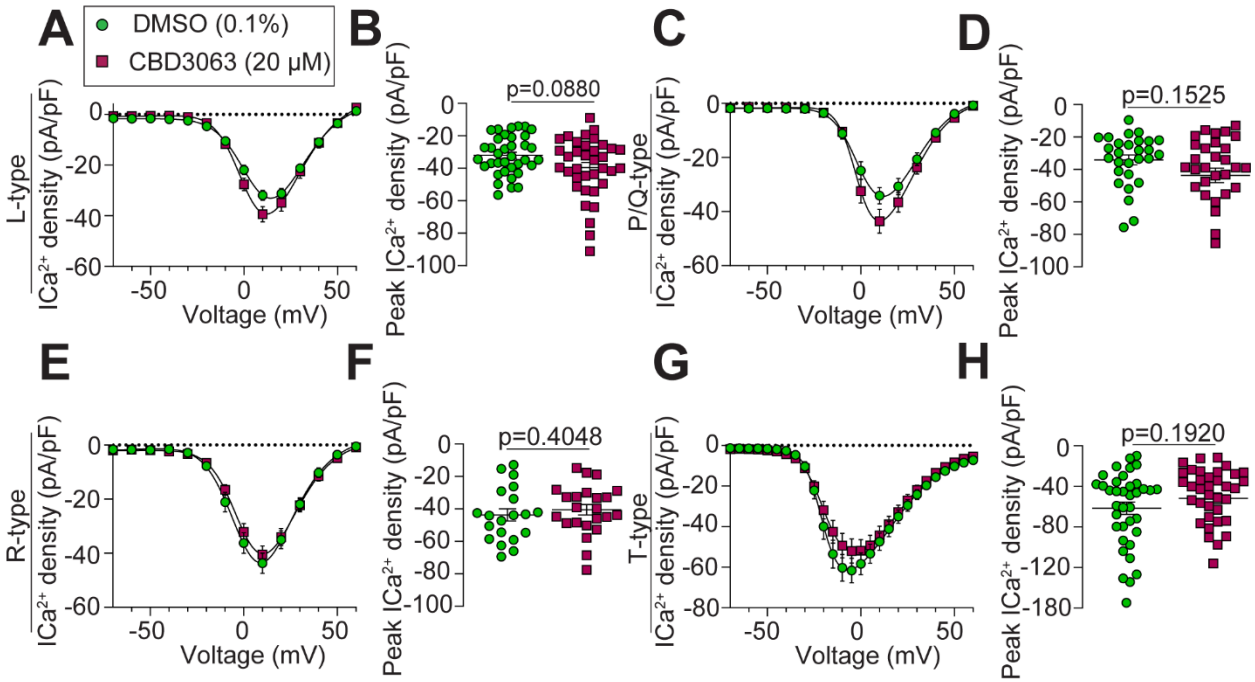

Figure S9. CBD3063 does not inhibit the activity of other voltage-gated calcium channel isoforms. (A, C, E, G) L-, P/Q-. R-, and T-type current density–voltage curves, respectively. No statistical significances were observed after applying Multiple Mann-Whitney tests. (B, D, F, H) Summary of bar graph showing peak L-, P/Q-. R-, and T-type calcium current densities (pA/pF), respectively. CBD3063 did not affect any of these currents after overnight incubation. *p* value as indicated; Mann-Whitney test. n=36 cells from seven separate rats (L-type); n=28-31 cells from five separate rats (P/Q-type); n=20-23 cells from three separate rats (R-type); n=37 cells from seven separate rats (T-type); Error bars indicate mean ± SEM; Half-maximal activation potential ($V_{1/2}$) and slope values (*k*) for activation and inactivation are presented in **Table S2**. See **Dataset 1** for full statistics.

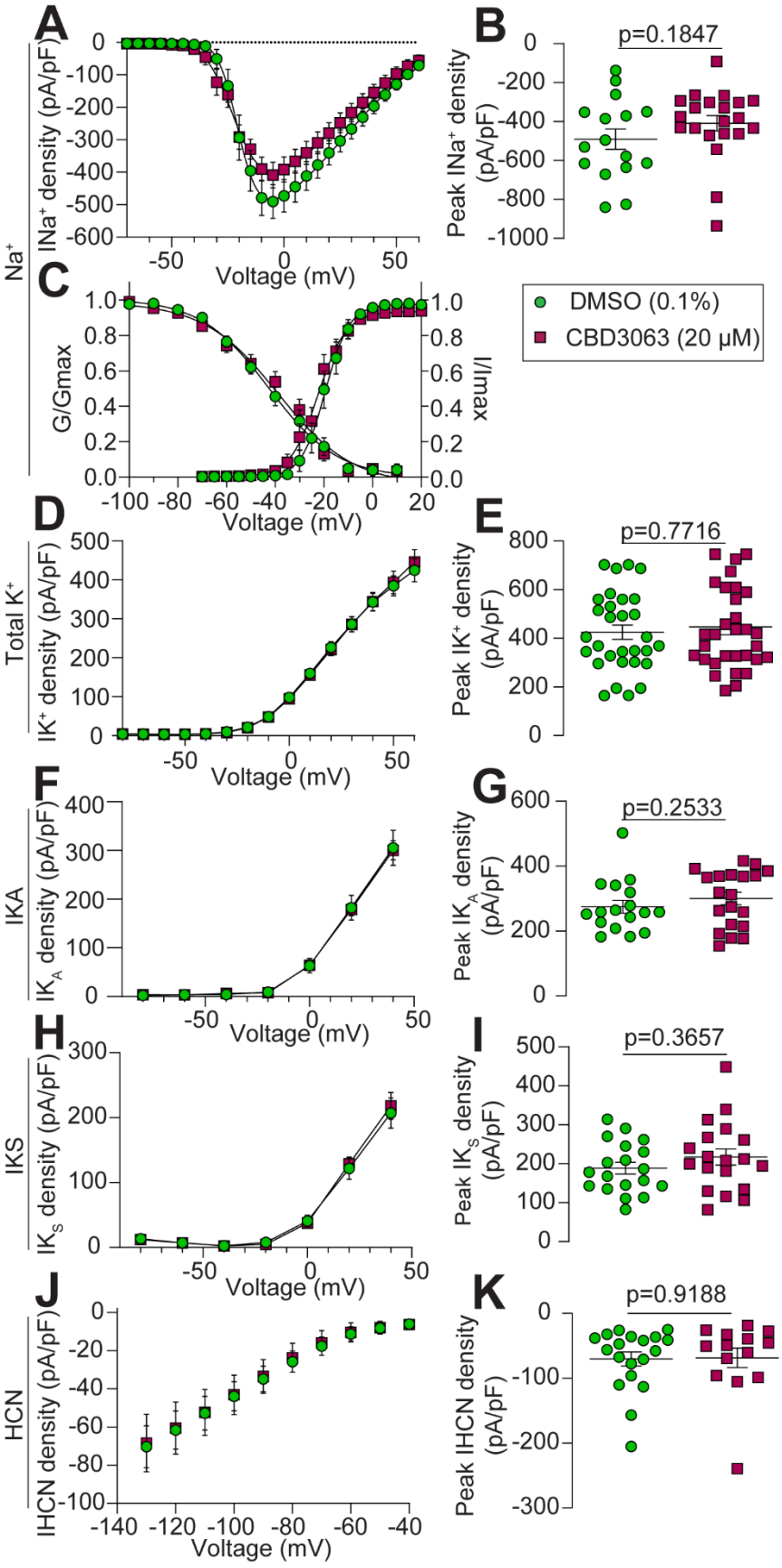
A
B
C
D
E
F
G
H
I
J
K
Na+
Total K+
IKA
IKS
HCN
INa+ density (pA/pF)
Peak INa+ density (pA/pF)
G/Gmax
I/Imax
Voltage (mV)
DMSO (0.1%)
CBD3063 (20 μM)
IK+ density (pA/pF)
Peak IK+ density (pA/pF)
IKA density (pA/pF)
Peak IKA density (pA/pF)
IKS density (pA/pF)
Peak IKS density (pA/pF)
IHCN density (pA/pF)
Peak IHCN density (pA/pF)
p=0.1847
p=0.7716
p=0.2533
p=0.3657
p=0.9188

938

Figure S10. Overnight incubation with CBD3063 does not affect total sodium, total potassium, IK_A, IK_S or HCN currents in DRG neurons. (A) Boltzmann fits for current density–voltage curve. Sodium currents were recorded from small– to medium–sized DRGs incubated overnight with 20 µM of CBD3063 as indicated in the figure. Currents were evoked by 150-ms pulse between −70 and +60 mV. (B) Summary of bar graph showing peak sodium current densities (pA/pF). *p* value as indicated; Mann-Whitney test. (C) Boltzmann fits for voltage-dependent activation and inactivation as shown. Half-maximal activation potential of activation and inactivation ($V_{1/2}$) and slope values (*k*) for activation and inactivation are presented in **Table 2**. n=16-21 cells from three separate rats. (D) Current density-voltage curves of total potassium currents recorded from sensory neurons in the presence of 0.1% DMSO or 20 µM CBD3063. Currents were evoked by 300-ms pulse between −80 and +60 mV. (E) Summary of peak potassium current densities (pA/pF). n=30-32 cells from four separate rats; *p* values as indicated; Mann-Whitney test. (F) Current density-voltage curves of IK_A potassium currents recorded from sensory neurons in the presence of 0.1% DMSO or 20 µM CBD3063. Currents were evoked by applying a 4-s pre-pulse to −100 mV followed by voltage steps of 500 milliseconds that ranged from −80 to +40 mV in +20-mV increments at 15-s intervals. (G) Summary of peak IK_A current densities (pA/pF). n=18-20 cells from two separate rats; *p* values as indicated; Mann-Whitney test. (H) Current density-voltage curves of IK_S potassium currents recorded from sensory neurons in the presence of 0.1% DMSO or 20 µM CBD3063. Currents were evoked by applying a conditioning 4-sec pre-pulse to −40 mV followed by voltage steps of 500 milliseconds that ranged from −80 to +40 mV in +20-mV increments at 15-s intervals. (I) Summary of peak IK_S current densities (pA/pF). n=19-20 cells from two separate rats; *p* values as indicated; Mann-Whitney test. (J) Current density-voltage curves of HCN currents recorded from sensory neurons in the presence of 0.1% DMSO or 20 µM CBD3063. Currents were evoked by applying 5000-millisecond voltage steps from −130 to -40 mV in 10-mV increments. (K) Summary of HCN peak current densities (pA/pF). n=14-19 cells from two separate rats; *p* values as indicated; Mann-Whitney test. Error bars indicate mean ± SEM. See **Dataset 1** for full statistics.

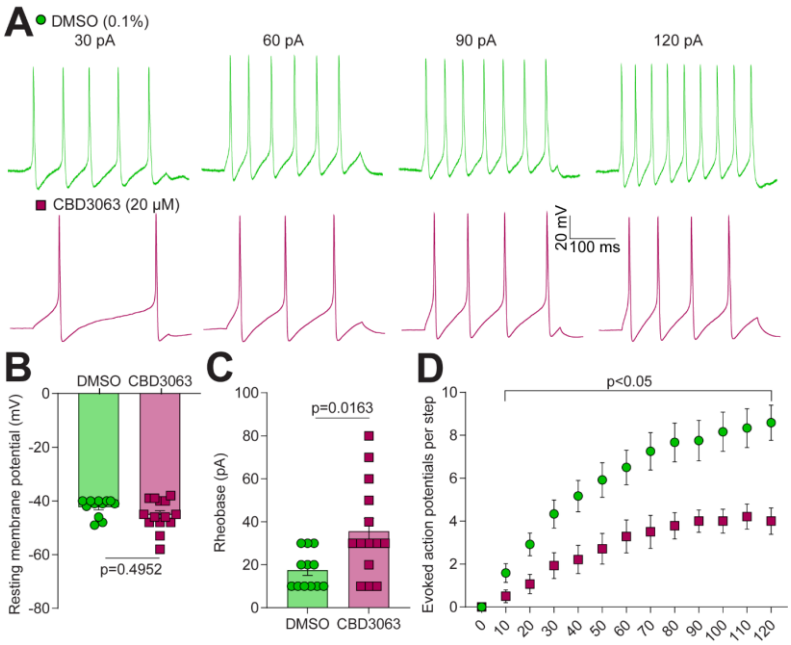

Figure S11. Sensory neuron excitability is decreased by overnight incubation of CBD3063. (A) Representative action potential traces in response to the indicated current injection steps obtained from rat DRG neurons treated with 0.1% DMSO (control) or 20 µM CBD3063. (B) Quantification of resting membrane potential in millivolts (mV) in the two conditions. (C) Quantification of the rheobase in the presence of DMSO or 20 µM CBD3063. (D) Summary of the number of evoked action potentials in response to current injection between 0-120 pA. N=12-14 cells from three separate rats; *p* value as indicated; Mann-Whitney test (B and C) and Multiple Mann-Whitney test. Error bars indicate mean ± SEM. See **Dataset 1** for full statistics.

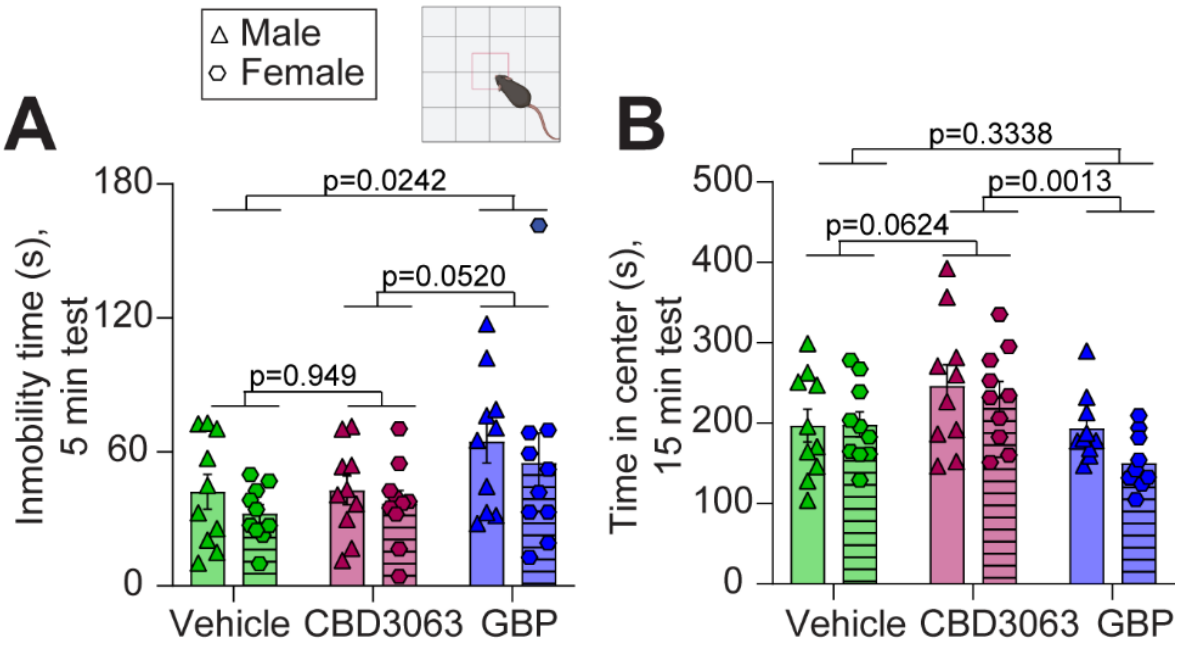

Figure S12. CDB3063 produced beneficial effects on anxiety-like and mobility-related behavior when compared with gabapentin. (A) Gabapentin (GBP; 30 mg/kg) produced sedative-like behaviors when compared with vehicle (10% DMSO in saline), and CBD3063 (10 mg/kg), as assessed by the duration of immobility in the Open Field during a 5-minute test, confirming the results found during the full 15-minute test (Figure 8G). (B) CBD3063 showed anxiolytic-like effects when compared with GBP and vehicle, as assessed by time spent in the center of the Open Field during a 15-minute test, confirming the results found during the first 5-minute of the test (Figure 8H). Injections were given intraperitoneal 2 hours before the test. N=10 mice per group. Results were compared using two-way ANOVA with time and treatment, as factors and Tukey post-hoc test. *p* values as indicated; Values are expressed as mean ± SEM. See **Dataset 1** for full statistics.

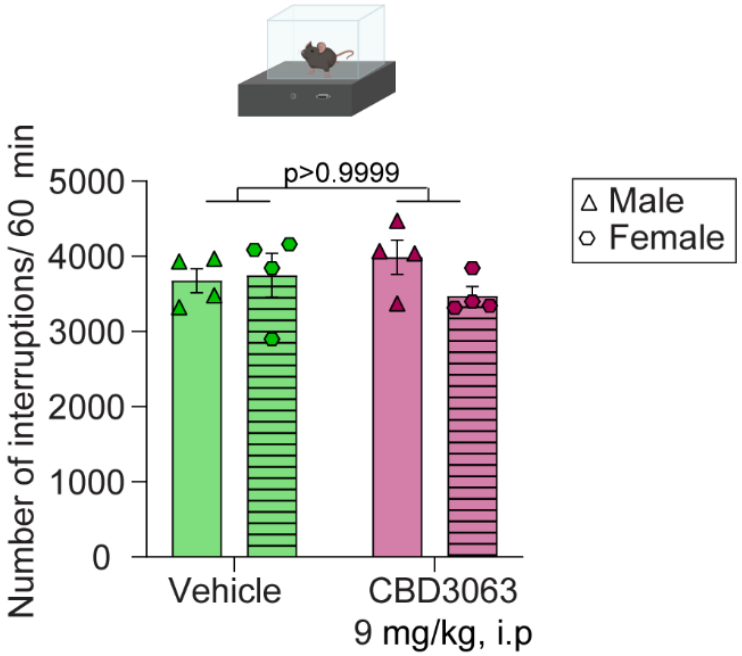

Figure S13. CBD3063 has no effect on locomotor activity in mice after i.p injection of paclitaxel (8 mg/kg). Values are expressed as mean ± SEM. Mice were tested 60 min after i.p. injection of CBD3063 (9 mg/kg) or saline and activity was measured for 60 min. CBD3063 (9 mg/kg, i.p) did not affect locomotor activity (Number of interruptions in 60 minutes) when compared to vehicle (saline)-treated mice. N=8 mice per group. Results were compared using two-way ANOVA with time and treatment, as factors and Tukey post-hoc test. *p* values as indicated; Values are expressed as mean ± SEM. See **Dataset 1** for full statistics.

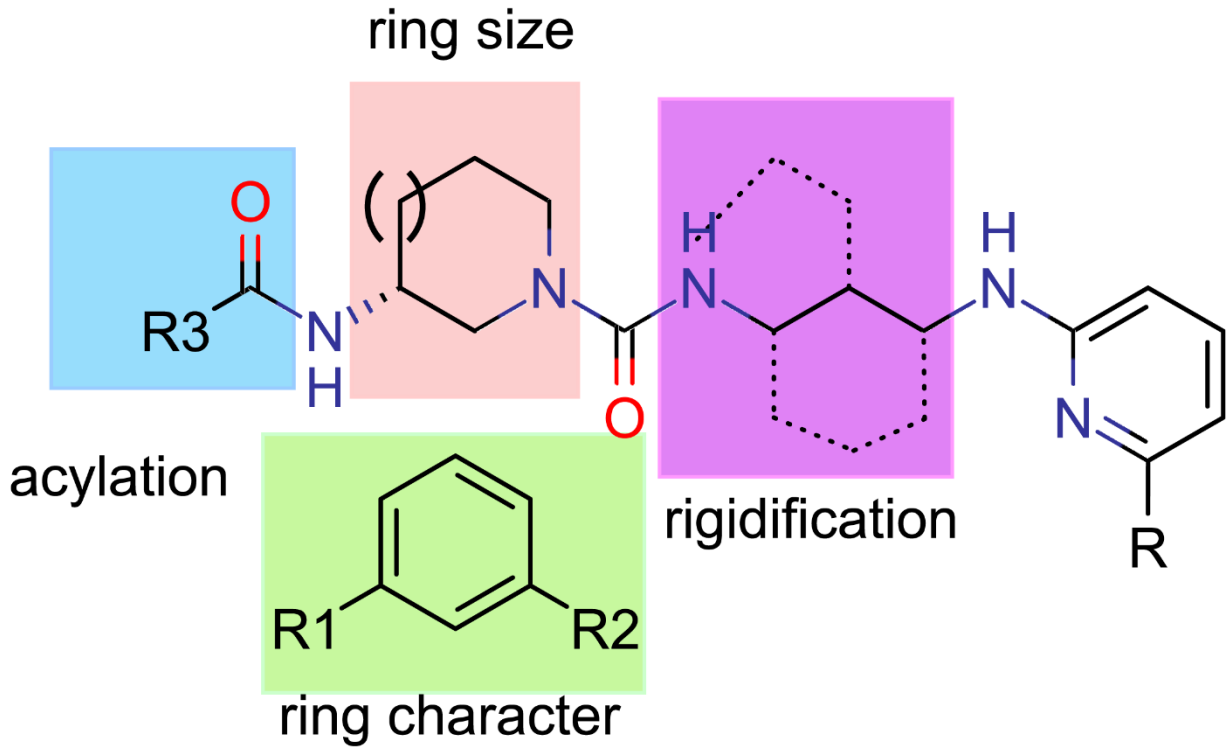

Figure S14. Molecule structure highlighting the areas to optimize. Blue, acylation. Pink, ring size. Magenta, rigidification. Green, ring character.

Table S1. Calculated properties of compounds inhibiting Ca^{+2} influx by more than 50%.

ID	IUPAC Name	Compound class	Mw	BBB	logS (7.4)	cLogP	HBD	HBA	RO5	NHOH	RotB	TPSA	QED
CBD3018	(Z)-N'-{4-[(3R,5S)-3,5-dimethylpiperidin-1-yl]butyl}-N,N''-dimethylguanidine	Guanidines	254.4	4.2	0.90	1.54	2	2	Y	2	5	39.7	0.44
CBD3026	ethyl N-benzoyl-(R)-arginine	Guanidines	306.4	2.2	0.00	0.61	4	4	Y	5	8	117.3	0.24
CBD3033	1-methyl-N-{3-[(5-methylpyridin-2-yl)amino]propyl}-6-oxopyridine-3-carboxamide	2-aminopyridylpropyl-carboxamides	300.4	4.0	-1.70	1.32	2	5	Y	2	6	76.0	0.79
CBD3038	8-fluoro-N-{3-[(5-methylpyridin-2-yl)amino]propyl}quinoline-2-carboxamide	2-aminopyridylpropyl-carboxamides	338.4	4.2	-4.10	3.31	2	4	Y	2	6	66.9	0.68
CBD3039	2-ethyl-5-isopropyl-N-{3-[(5-methylpyridin-2-yl)amino]propyl}pyrazole-3-carboxamide	2-aminopyridylpropyl-carboxamides	329.4	4.2	-2.90	2.96	2	5	Y	2	8	71.8	0.73
CBD3062	1-[(3S)-2-oxoazepan-3-yl]-3-[3-(pyridin-2-ylamino)propyl]urea	2-aminopyridylpropylureas	305.4	2.9	-1.90	0.85	4	4	Y	4	6	95.2	0.59
CBD3063	(3R)-3-acetamido-N-[3-(pyridin-2-ylamino)propyl]piperidine-1-carboxamide	2-aminopyridylpropylureas	319.4	3.8	-2.00	1.19	3	4	Y	3	6	86.4	0.69
CBD3065	N'-benzyl-N-[3-(3,4-dihydro-1H-isoquinolin-2-yl)propyl]guanidine	Guanidines	322.5	4.6	0.00	2.75	3	2	Y	3	6	51.2	0.44
CBD3074	N-[3-(1,3-dihydroisoindol-2-yl)propyl]-N'-[(2-methoxyphenyl)methyl]guanidine	Guanidines	338.5	4.2	0.00	2.72	3	3	Y	3	7	60.4	0.41

Compounds identified as active in calcium imaging (**Figure S3**). Mw, molecular weight (Da); BBB score, indicates probability of compound having CNS exposure where scores in the range [4-6] correctly predicted 90.3% of CNS drugs (32); LogS(7.4), predicted solubility (M) at pH 7.4; cLogP, predicted lipophilicity coefficient in octanol/water; HBD, number of hydrogen-bond donors; HBA, number of hydrogen bond acceptors; RO5, binary (Y/N) assignment of complying with Lipinski rule-of-5 (33); NHOH, number of polar NH and OH hydrogens; RotB, number of rotatable bonds; TPSA, topological polar surface area ($Å^2$); QED, Quantitative Estimate of Druglikeness where a score of 1 indicates all properties are favorable (34). Properties calculated with RDKit and ChemAxon modules.

Table S2. Gating properties of ionic currents recorded from rat DRG neurons in the presence of CBD3063.

	DMSO	CBD3063
Total Ca^{2+} currents (Figure S5)		
Activation		
$V_{1/2}$	-0.665 ± 1.091 (13)	0.971 ± 2.338 (16)
k	7.429 ± 0.991 (13)	11.004 ± 2.181 (16)
Inactivation		
$V_{1/2}$	-17.081 ± 2.647 (13)	-20.944 ± 3.182 (16)
k	-10.916 ± 2.186 (13)	-14.132 ± 2.880 (16)
N-type Ca^{2+} currents (Figure 2)		
Activation		
$V_{1/2}$	-2.234 ± 0.421 (32)	-2.446 ± 0.471 (36)
k	5.184 ± 0.369 (32)	5.822 ± 0.410 (36)
Inactivation		
$V_{1/2}$	-21.190 ± 1.697 (32)	-22.482 ± 2.389 (36)
k	-15.833 ± 1.293 (32)	-17.446 ± 1.868 (36)
N-type Ca^{2+} currents (Male rats; figure S7)		
Activation		
$V_{1/2}$	3.064 ± 0.480 (16)	2.549 ± 0.383 (20)
k	4.868 ± 0.404 (16)	5.204 ± 0.330 (20)
Inactivation		
$V_{1/2}$	-21.669 ± 3.247 (16)	-18.878 ± 2.118 (20)
k	16.679 ± 2.491 (16)	15.047 ± 1.531 (20)
N-type Ca^{2+} currents (Acute application; figure S8)		
Activation		
$V_{1/2}$	-1.418 ± 0.288 (36)	0.586 ± 0.500 (30)
k	4.667 ± 0.266 (36)	5.878 ± 0.443 (30)
Inactivation		
$V_{1/2}$	-20.536 ± 1.253 (36)	-22.078 ± 1.418 (30)
k	-12.349 ± 0.986 (36)	-12.093 ± 1.155 (30)
L-type Ca^{2+} currents (Figure S9)		
Activation		
$V_{1/2}$	0.274 ± 0.513 (36)	-1.957 ± 0.402 (36)
k	6.423 ± 0.449 (36)	5.267 ± 0.355 (36)
Inactivation		
$V_{1/2}$	-13.503 ± 0.890 (36)	-15.370 ± 0.933 (36)
k	-9.371 ± 0.750 (36)	-8.188 ± 0.803 (36)
P/Q-type Ca^{2+} currents (Figure S9)		
Activation		
$V_{1/2}$	-1.644 ± 0.527 (28)	-2.086 ± 0.363 (31)
k	5.301 ± 0.469 (28)	4.566 ± 0.324 (31)
Inactivation		
$V_{1/2}$	-14.833 ± 1.217 (28)	-13.091 ± 0.791 (31)
k	-10.130 ± 1.028 (28)	-9.191 ± 0.666 (31)
R-type Ca^{2+} currents (Figure S9)		
Activation		
$V_{1/2}$	-4.688 ± 0.615 (20)	-3.688 ± 0.625 (23)
k	6.365 ± 0.519 (20)	6.421 ± 0.524 (23)
Inactivation		
$V_{1/2}$	-24.330 ± 2.384 (20)	-18.422 ± 1.461 (23)
k	-17.194 ± 2.251 (20)	-12.260 ± 1.256 (23)
T-type Ca^{2+} currents (Figure S9)		
Activation		
$V_{1/2}$	-20.044 ± 0.421 (37)	-19.529 ± 0.647 (37)
k	4.800 ± 0.368 (37)	6.684 ± 0.581 (37)
Inactivation		
$V_{1/2}$	-40.758 ± 1.046 (37)	-40.757 ± 1.129 (37)
k	-11.305 ± 0.994 (37)	-11.606 ± 1.078 (37)
Na^{+} currents (Figure S10)		
Activation		
$V_{1/2}$	-19.288 ± 0.625 (16)	-22.340 ± 0.686 (21)
k	4.955 ± 0.547 (16)	5.752 ± 0.606 (21)
Inactivation		
$V_{1/2}$	-42.563 ± 1.843 (16)	-38.767 ± 2.083 (21)
k	-14.098 ± 1.895 (16)	-15.283 ± 2.173 (21)

Values are means ± SEM calculated from fits of the data from the indicated number of individual cells (in parentheses) to the Boltzmann equation; $V_{1/2}$ midpoint potential (mV) for voltage-dependent of activation or inactivation; *k*, slope factor. Data were analyzed with Mann-Whitney test.

SI References

1. S. Cai *et al.*, Selective targeting of NaV1.7 via inhibition of the CRMP2-Ubc9 interaction reduces pain in rodents. *Sci Transl Med* **13**, eabh1314 (2021).
2. Y. Zheng *et al.*, Tuning microtubule dynamics to enhance cancer therapy by modulating FER-mediated CRMP2 phosphorylation. *Nat Commun* **9**, 476 (2018).
3. D. A. Case *et al.* (2018) AMBER 2018. (Univesity of California, San Francisco).
4. A. W. Götz *et al.*, Routine Microsecond Molecular Dynamics Simulations with AMBER on GPUs. 1. Generalized Born. *J Chem Theory Comput* **8**, 1542-1555 (2012).
5. R. Salomon-Ferrer, A. W. Götz, D. Poole, S. Le Grand, R. C. Walker, Routine Microsecond Molecular Dynamics Simulations with AMBER on GPUs. 2. Explicit Solvent Particle Mesh Ewald. *J Chem Theory Comput* **9**, 3878-3888 (2013).
6. J. A. Maier *et al.*, ff14SB: Improving the Accuracy of Protein Side Chain and Backbone Parameters from ff99SB. *J Chem Theory Comput* **11**, 3696-3713 (2015).
7. D. Kozakov, K. H. Clodfelter, S. Vajda, C. J. Camacho, Optimal clustering for detecting near-native conformations in protein docking. *Biophys J* **89**, 867-875 (2005).
8. D. Rajamani, S. Thiel, S. Vajda, C. J. Camacho, Anchor residues in protein-protein interactions. *Proc Natl Acad Sci U S A* **101**, 11287-11292 (2004).
9. D. R. Koes, C. J. Camacho, ZINCPharmer: pharmacophore search of the ZINC database. *Nucleic Acids Res* **40**, W409-414 (2012).
10. P. C. Hawkins, A. G. Skillman, G. L. Warren, B. A. Ellingson, M. T. Stahl, Conformer generation with OMEGA: algorithm and validation using high quality structures from the Protein Databank and Cambridge Structural Database. *J Chem Inf Model* **50**, 572-584 (2010).
11. E. T. Dustrude *et al.*, Hierarchical CRMP2 posttranslational modifications control NaV1.7 function. *Proc Natl Acad Sci U S A* **113**, E8443-E8452 (2016).
12. K. Gomez *et al.*, Stereospecific Effects of Benzimidazolonepiperidine Compounds on T-Type Ca(2+) Channels and Pain. *ACS Chem Neurosci* 10.1021/acschemneuro.2c00256 (2022).
13. S. S. Bellampalli *et al.*, Betulinic acid, derived from the desert lavender Hyptis emoryi, attenuates paclitaxel-, HIV-, and nerve injury-associated peripheral sensory neuropathy via block of N- and T-type calcium channels. *Pain* **160**, 117-135 (2019).
14. A. Moutal *et al.*, Homology-guided mutational analysis reveals the functional requirements for antinociceptive specificity of collapsin response mediator protein 2-derived peptides. *Br J Pharmacol* **175**, 2244-2260 (2018).
15. A. Moutal *et al.*, Dissecting the role of the CRMP2-neurofibromin complex on pain behaviors. *Pain* **158**, 2203-2221 (2017).
16. A. Moutal *et al.*, Studies on CRMP2 SUMOylation-deficient transgenic mice identify sex-specific Nav1.7 regulation in the pathogenesis of chronic neuropathic pain. *Pain* **161**, 2629-2651 (2020).
17. Z. P. Feng *et al.*, Residue Gly1326 of the N-type calcium channel alpha 1B subunit controls reversibility of omega-conotoxin GVIA and MVIIA block. *J Biol Chem* **276**, 15728-15735 (2001).
18. R. Newcomb *et al.*, Selective peptide antagonist of the class E calcium channel from the venom of the tarantula Hysterocrates gigas. *Biochemistry* **37**, 15353-15362 (1998).
19. I. M. Mintz *et al.*, P-type calcium channels blocked by the spider toxin omega-Aga-IVA. *Nature* **355**, 827-829 (1992).
20. W. Choe *et al.*, TTA-P2 is a potent and selective blocker of T-type calcium channels in rat sensory neurons and a novel antinociceptive agent. *Mol Pharmacol* **80**, 900-910 (2011).
21. Y. Dou *et al.*, Orai1 Plays a Crucial Role in Central Sensitization by Modulating Neuronal Excitability. *J Neurosci* **38**, 887-900 (2018).
22. D. Bagdas, S. D. AlSharari, K. Freitas, M. Tracy, M. I. Damaj, The role of alpha5 nicotinic acetylcholine receptors in mouse models of chronic inflammatory and neuropathic pain. *Biochem Pharmacol* **97**, 590-600 (2015).
23. Y. Imamura, H. Kawamoto, O. Nakanishi, Characterization of heat-hyperalgesia in an experimental trigeminal neuropathy in rats. *Exp Brain Res* **116**, 97-103 (1997).
24. T. L. Yaksh, T. A. Rudy, Chronic catheterization of the spinal subarachnoid space. *Physiol Behav* **17**, 1031-1036 (1976).
25. S. R. Chaplan, F. W. Bach, J. W. Pogrel, J. M. Chung, T. L. Yaksh, Quantitative assessment of tactile allodynia in the rat paw. *J Neurosci Methods* **53**, 55-63 (1994).

26. C. Y. Liu *et al.*, The role of large-conductance, calcium-activated potassium channels in a rat model of trigeminal neuropathic pain. *Cephalalgia* **35**, 16-35 (2015).
27. A. Narula, J. S. McCormick, Spontaneous duodenocolic fistula. *J R Coll Surg Edinb* **35**, 253-254 (1990).
28. R. A. Bevins, J. Besheer, Object recognition in rats and mice: a one-trial non-matching-to-sample learning task to study 'recognition memory'. *Nat Protoc* **1**, 1306-1311 (2006).
29. M. I. Ferdousi *et al.*, Characterization of pain-, anxiety-, and cognition-related behaviors in the complete Freund's adjuvant model of chronic inflammatory pain in Wistar-Kyoto rats. *Front Pain Res (Lausanne)* **4**, 1131069 (2023).
30. R. Benoliel, A. Wilensky, M. Tal, E. Eliav, Application of a pro-inflammatory agent to the orbital portion of the rat infraorbital nerve induces changes indicative of ongoing trigeminal pain. *Pain* **99**, 567-578 (2002).
31. B. P. Vos, A. M. Strassman, R. J. Maciewicz, Behavioral evidence of trigeminal neuropathic pain following chronic constriction injury to the rat's infraorbital nerve. *J Neurosci* **14**, 2708-2723 (1994).
32. M. Gupta, H. J. Lee, C. J. Barden, D. F. Weaver, The Blood-Brain Barrier (BBB) Score. *J Med Chem* **62**, 9824-9836 (2019).
33. C. A. Lipinski, Lead- and drug-like compounds: the rule-of-five revolution. *Drug Discov Today Technol* **1**, 337-341 (2004).
34. G. R. Bickerton, G. V. Paolini, J. Besnard, S. Muresan, A. L. Hopkins, Quantifying the chemical beauty of drugs. *Nat Chem* **4**, 90-98 (2012).